Numerically Generating Topology of the Liner Finish in Internal Combustion Engines

by
Renze Wang

B.Sc., Electronics Engineering and Computer Science
Peking University, 2012

Submitted to the MIT Department of Materials Science and Engineering and Department of Mechanical Engineering in Partial Fulfillment of the Requirements for the Degrees
of
Master of Science in Materials Science and Engineering and
Master of Science in Mechanical Engineering

at the
Massachusetts Institute of Technology

September 2015

Signature of Author: Signature redacted
Department of Materials Science and Engineering
August 14, 2015

Certified by: Signature redacted
Dr. Tian Tian
Principal Research Engineer, Department of Mechanical Engineering
Thesis Supervisor

Certified by: Signature redacted
Polina Anikeeva
Professor, Department of Materials Science and Engineering
Thesis Reader

Accepted by: Signature redacted
Donald Sadoway
Professor of Materials Science and Engineering
Chair, Departmental Committee on Graduate Students

Accepted by: Signature redacted
David E.Hardt
Professor of Mechanical Engineering
Chair, Departmental Committee on Graduate Students

Numerically Generating Topology of the Liner Finish in Internal Combustion Engines

by

Renze Wang

Submitted to the Department of Materials Science and Engineering and Department of Mechanical Engineering on August 14, 2015 in Partial Fulfillment of the Requirements for the Degree of Double Masters of Science in Materials Science and Engineering, and Mechanical Engineering

Abstract

Internal combustion (IC) engines are broadly utilized today. The friction caused by piston rings in IC engines contributes around 20% of the mechanical friction losses. The liner finish is the most critical parameter to define the tension and other design parameters of the piston rings for proper sealing. This work is focused on developing numerical approaches to generating liner finishes based on certain values of topology parameters. The generated surface is able to simulate the lubrication and dry contact behaviors of the original surface, so that the method is used to study the effects of various topology parameters on friction losses.

First, methods to analyze, generate, test, and compare honed liner surfaces have been developed. The algorithm to analyze the topology parameters of honed surfaces is described. The honed surfaces are numerically generated and compared with the experimental data. Moreover, the topological variables are changed and the corresponding friction behaviors are studied. The relations between topology variables and friction losses are illustrated. We also developed a quantitative relation between two ISO standards describing the honed liner finish, so that the manufacturing industry can use the surface generation method in convenience.

Second, attempts were made to simulate the break-in processes for honed liner finish. Measured and numerically generated surfaces are simulated and compared. The friction and pressure behaviors for lightly and heavily worn surfaces are compared with experimental data. Moreover, by tuning the worn parameters, the friction effective mean pressure (FMEP) curve can match the experimental data.

Finally, the algorithm to numerically generate thermally sprayed liner finish is described. The hydrodynamic and dry contact friction behaviors for generated surfaces are compared with experimental data. Critical topology parameters are tuned and their effects on friction losses are studied. Moreover, the effects of the pores created by the plasma spraying processes on the lubrication behaviors are simulated.

Thesis Supervisor:

Dr. Tian Tian, Department of Mechanical Engineering

Acknowledgements

There are many people who I would like to thank for their contributions to this research, and to my study at MIT for the past three years. These contributions gave me many opportunities for developments on both personal and professional level.

First of all, I would like to thank my advisor, Dr. Tian Tian, for his support and guidance throughout my research and life. I have learned a great deal through my exposure to his depth of knowledge, insight, experience and logical approaches to solving problems. I would also like to thank my peer workers Kai Liao and Dallwoo Kim, who collected the experimental data I used in the thesis. I would like to thank Haijie Chen and Yang Liu as well who I carry on this project from. Their work and knowledge helped me understand and develop the model theoretically. I would like to thank my thesis reader, Professor Polina Anikeeva, who gave me great support in my graduate study.

This work is sponsored by the consortium on lubrication in internal combustion engines, whose members are Daimler, Mahle, PSA, Renault, Toyota, Volkswagen, Volvo and Shell for their financial support, and more specifically, their representatives, Hans-Juergen Fuesser, Matthias Martin, Rolf-Gerhard Fiedler, Remi Rabute, Erich Rabassa, Franck Choukroun, Bengt Olsson, Paulo Urzua Torres, Tom Shieh, Shohei Nomura, Brian Papke, Scott Rappaport, Steve Przesmitzki and others for their continuous encouragement over the years, and for sharing their extensive experience with me. Our regular meetings provided not only a motivation for completing the work, but also an invaluable opportunity to share knowledge and obtain constructive feedback. I would especially like to thank MAHLE for providing the rings, Volkswagen and Daimler for providing their liners and Shell for providing the lubricant oil. Without their help, we cannot finish the experiment.

I would also like to thank the members of the Sloan Automotive Laboratory for their support and friendship. In particular I would like to thank students of the Lubrication Consortium and my office mates, Yang Liu, Camille Baelden, Mathieu Picard, Tianshi Fang, Qing Zhao, Eric Zanghi, Pasquale Totaro, Zachary Westerfield for their help to make the stressful time relieving.

Finally, I would like to thank my friends and family for their support throughout my time here.

Table of Contents

Table of Figures

Chapter One

Chapter Two

Chapter Three

Chapter Four

1. Introduction

1.1 Project Motivation

Internal combustion (IC) engines are broadly utilized today. They consume great amount of oil while emit CO_2 and other harmful gas. Therefore it is important to study the operation processes of IC engines, and design more efficient ones.

As Figure 1.1 [1] shown, for a standard diesel automotive, around 10% of the total fuel energy is wasted on the mechanical friction. The friction caused by piston rings and liner finishes contributes around 20% of the mechanical friction losses. The oil control rings contribute more than half of the piston ring pack friction losses. Therefore, it is important to study the friction behaviors between oil control rings and the piston liners.

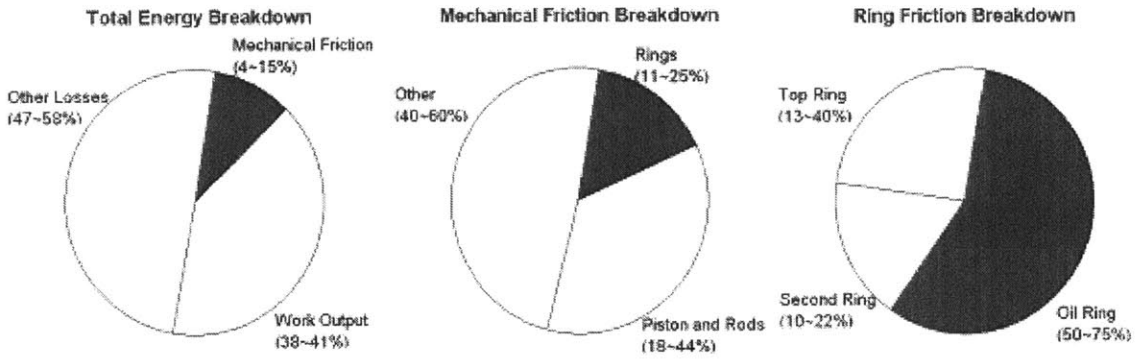

Figure 1. 1: Breakdown of Total Diesel Engine Energy, Mechanical Friction and Ring Pack Friction [1]

Cylinder (liner) surface topology plays important roles in studying hydrodynamic and dry contact frictions, oil consumptions, and engine performances [2-5]. For numerical simulation of the tribological behaviors of engineering surfaces, such as contact problem, hydrodynamic and elastohydrodynamic lubrication, the three dimensional surface topology is a critical input [6-10]. It can be achieved either by profilometer or by numerical simulation of the surfaces. The numerical simulation methods are simpler, less time-consuming, cheaper, and more flexible. It can eliminate the hardware and software requirements. It also avoids the complicated post measurement processes, such as removing wavelengths, interpolating blank points. Moreover, we will see that it avoids fake spikes caused by measurement error.

The numerical methods to generate two step honed surfaces are broadly studied by researchers [11-14]. However, there are still plenty of issues necessary to be studied. First of all, though the numerical method is well described, it is not combined with deterministic and engine cycle models to study the impacts of various topological parameters on the engine operation efficiency and oil consumption. Moreover, the advantage of numerical methods for avoiding measurement error is not addressed. Second, most studies focus on two step honed liner surfaces, while the state-of-art sprayed surfaces are not well studied. Third, the geometric parameters used for generating surfaces are different from automotive industry, therefore cannot be directly used for design. Last but not least, not much research focuses on the surface worn processes, which are important to engine reliability.

1.2 Piston Ring Pack

The piston rings in the combustion chamber of an IC engine are some separate rings that can fit into the grooves between the piston and liner surface. The major function of the piston rings is to seal the combustion chambers and prevent oil and gas transfer between the chamber and crank case, therefore decrease oil consumption. On the other hand, piston rings increase the friction losses between the piston liners and cylinders, thus decrease engine efficiency [15]. A better design of piston rings and liner finishes can improve engine efficiency while decrease oil consumption.

A standard industry used piston ring pack usually consists three rings. As Figure 1.2 shown, from top to bottom, they are top rings (compression rings), second rings (scraper rings), and oil control rings (OCRs).

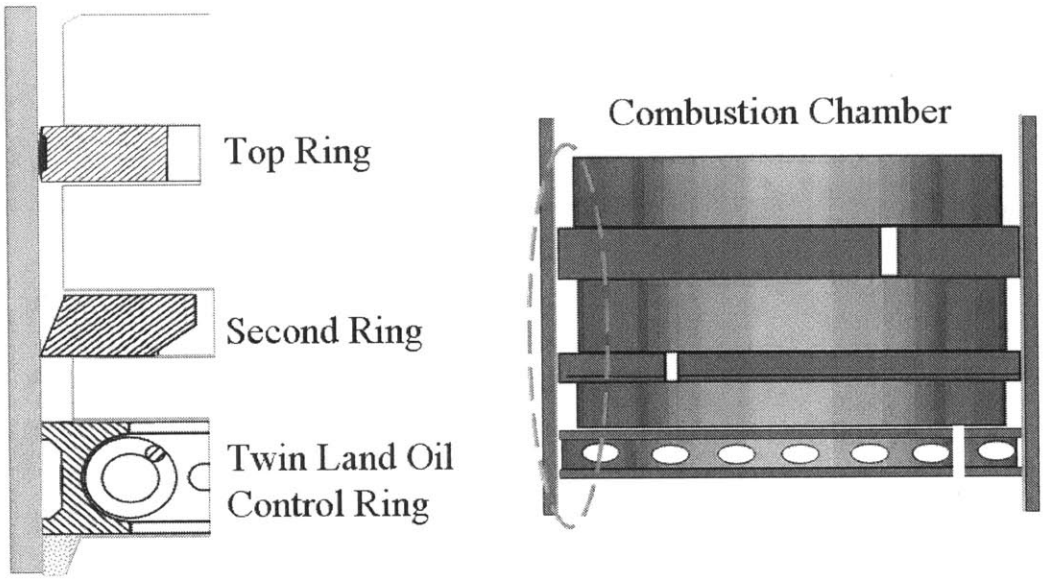

Figure 1. 2: Piston Ring Pack in Combustion Chamber of an Internal Combustion Engine

The design of twin land oil control ring (TLOCR) is broadly utilized in diesel engines [4]. Large normal force is exerted by the TLOCR spring so that TLOCR can effectively seal the oil in the crank case, which results in large friction losses. If the oil thickness increases, the oil consumption might increase while friction losses will decrease. The detailed study of engine operation is needed, so that people could make a good trade-off between oil consumption and engine efficiency.

1.3 Plateau-honed Cylinder Liner

One of the state-of-art liner manufacturing techniques is plateau-honing process. This process guarantees reproducibility and efficient productivity. The process includes three stages. First, the cylinder bore is roughly honed. Then the second honing will create the valley part with grooves. Finally, the third honing stage creates the plateau part with much smaller roughness compared with the valley [16, 17].

As Figure 1.3 shown, the typical cylinder liner manufactured by the plateau-honing process consists of the plateau and valley parts. The plateau part has smoother structure, while the valley part has the cross-hatch groove patterns, which are important to the lubrication behavior.

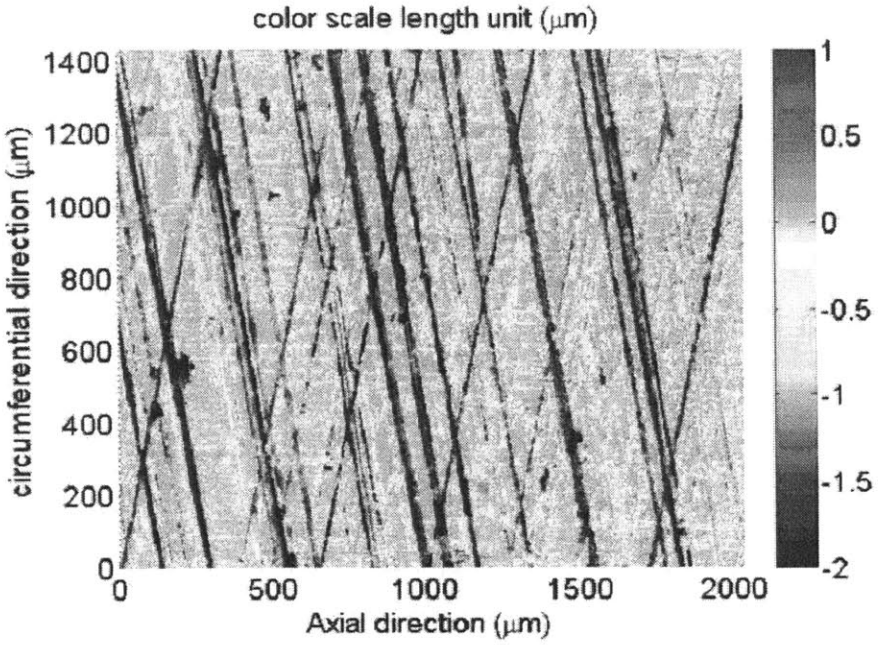

Figure 1. 3: A Typical break-in Cylinder Liner Geometry Profile [18]

1.3.1 ISO Standards for Honed Liner Surfaces

There are two independent sets of ISO standards describing the geometry of the liner surfaces [19-23]. Figure 1.4 shows the ISO 13565-2 standard, which is broadly used in manufacturing industry. The parameters are calculated using material ratio curve of the liner surface. The parameters can be determined include: the reduced peak height Rpk, the reduced valley depth Rvk, the core roughness depth Rk, the material ratios determined by the regression line separating the core roughness (40% of total roughness) from the material side (Rmr1) and free from the material side (Rmr2) [24].

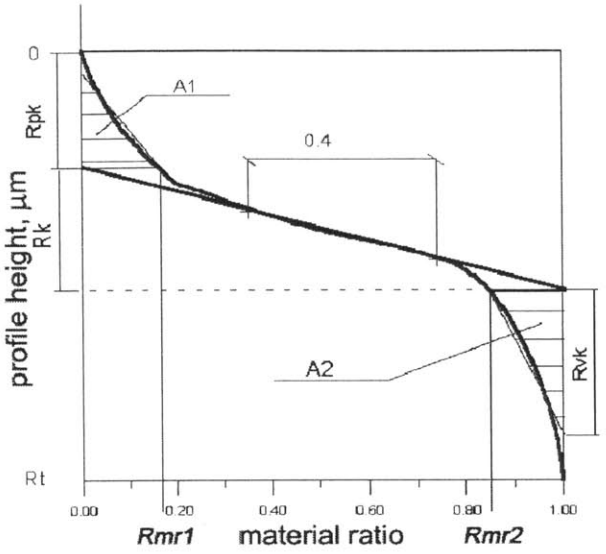

Figure 1. 4: ISO 13565-2 Standard Used to Describe Liner Geometry [20]

Figure 1.5 shows ISO 13565-3 standard, which can also be utilized to characterize the surface liner geometry. The parameters of this standard are used as input for liner surface generation algorithms [2]. In this approach, the plateau and valley parts can be well defined. The parameters are calculated by the normalized material ratio curve. The slopes of the two straight lines represent the root mean square (RMS) of plateau and valley respectively. Pd corresponds to the mean height difference between plateau and valley parts.

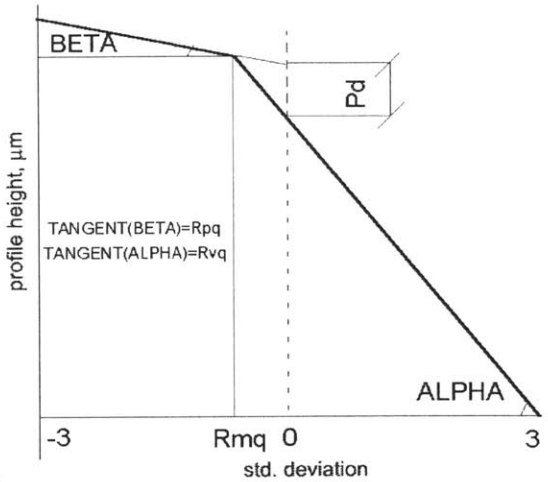

Figure 1. 5: ISO 13565-3 Standard Used to Describe Liner Geometry [20]

In manufacturing industry, ISO 13565-2 standard is broadly used. In contrast, for surface generation algorithm, the input should be ISO 13565-3. Therefore, the study of parameter connections between the two standards is needed. Some analytic researches have been conducted [19, 20], but none of them shows the quantitative relations.

1.3.2 Algorithms for Honed Liner Surfaces Generation

Besides the root mean square (RMS) for plateau roughness, RMS for valley roughness, and plateau ratio that can be obtained from ISO 13565-2 and material ratio curve mentioned above, one still needs the autocorrelation lengths of plateau and valley part in two orthogonal directions to generate a surface [12]. All these parameters can be obtained from a measured surface with proper methods.

For discrete finite points (assume N points), the autocorrelation function can be defined as [25]:

$$C_r = \frac{1}{N}\sum_{S=0}^{N-1} Z_s Z_{s+r}$$

Where Cr is the autocorrelation function, and Z is the roughness height. For the boundary conditions, we have:

$$Z_{s+r} = Z_{s+r-N}, for\ s + r \geq N$$

$$C_r = C_{N-r} = \frac{N-r}{N} R_r + \frac{r}{N} R_{N-r}$$

ACF of one surface is also the reverse Fourier transform of the spectral density of the surface, which means:

$$C_r = \sum_{k=0}^{N-1} S_k exp(\frac{i2\pi kr}{N})$$

where S_k is the spectral density. Figure 1.6 shows the autocorrelation function of a sample piston liner. Autocorrelation length corresponds to the distance where ACF drops to 10% from its largest value.

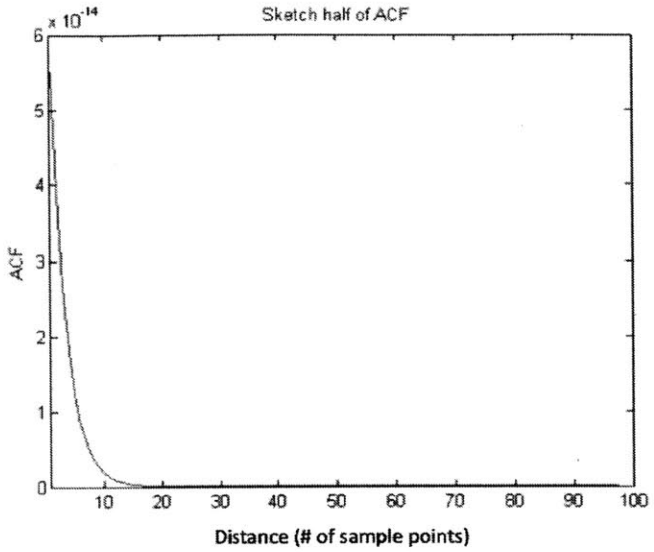

Figure 1. 6: Sample of the Autocorrelation Function (ACF).

Once all parameters are obtained from the specimen liner surfaces (the algorithms will be described in Chapter Two), new surfaces can be numerically generated.

First of all, the ACF need to be generated based on the autocorrelation lengths achieved from the original surface. It was already suggested by many researchers that ACF of cylinder surface is assumed to have an exponential form [12]. Therefore, there is a relation between ACF and autocorrelation lengths shown below:

$$R(x,y) = sigma^2 * \exp(2.3 \sqrt{(x/xlen)^2 + (y/ylen)^2})$$

where R is the ACF, sigma is the root mean square (RMS) of the corresponding parts of the original surface (can be achieved by statistical methods), xlen and ylen are the autocorrelation lengths in x and y directions.

After generating the ACF, the spectral power of the generated surface can be easily achieved by conducting FFT on the ACF, like the following shown,

$$S_{k,l} = \frac{1}{MN} \sum_{r=0}^{M1} \sum_{s=0}^{N1} R_{r,s} \exp(i2 \quad [\frac{kr}{M} + \frac{ls}{N}])$$

$$k = 0,1,...,(M\ 1)$$

$$l = 0,1,...,(N\ 1)$$

where S is the spectral power, M and N is the size of the surface, and R corresponds to ACF. Then utilizing inverse FFT and random variable, we can get the height information of the generated surface (this is what we need), like the following shown,

$$z_{p,q} = \sum_{k=0}^{M1} \sum_{l=0}^{N1} \sqrt{S_{k,l}} \exp(i2 \quad [\quad _{k,l} + \frac{kp}{M} + \frac{lq}{N}])$$

$$p = 0,1,2,\ldots,(M\ 1)$$

$$q = 0,1,2,\ldots,(N\ 1)$$

where z is the height (roughness) of the generated surface, φ is a set of independent random phase angles uniformly distributed between 0 and 2π. Eventually, each generated part (valley and plateau) is combined together based on their mean height difference achieved from the original surface.

1.3.3 Surface Measurement Error

Based on the efficiency and accuracy requirements, three methods are usually utilized to measure the roughness profile of piston liners – stylus profiler method, white light interferometry (WLI) method, and confocal microscopy method [26, 27].

Stylus profiler is a contacting method as figure 1.7 shown. The vertical motion of the stylus is converted to an electrical signal by a transducer, which leads to high vertical resolution. However, the lateral resolution is limited by the size of the stylus tip. Since mechanical contacts are required for this method, the surfaces may be damaged during measurements by the stylus [28].

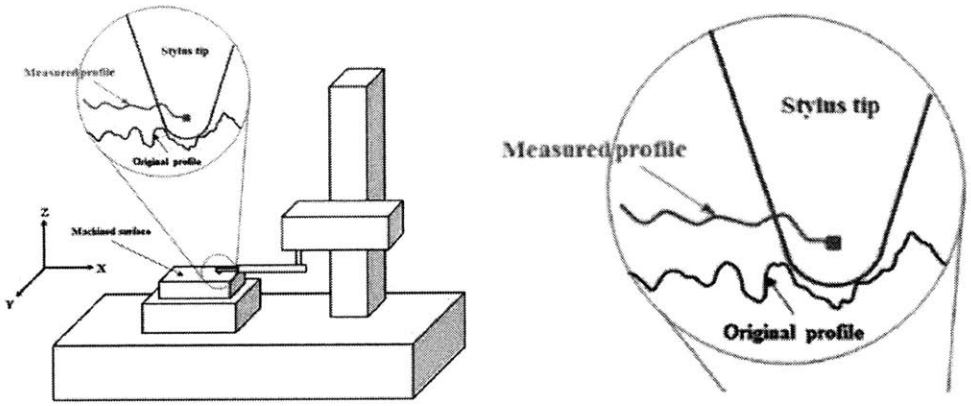

Figure 1. 7: Schematic Drawing of Stylus Profiler Method [28]

Confocal microscope and WLI microscope use optical (i.e. non-contacting) method to measure the roughness profiles [29-34]. Figure 1.8 shows the workflow of confocal microscopy. It uses laser and pinhole to illuminate the measured surface, and then collect the signal of incident and reflect light. The intensity changes when the roughness height changes. This method does not mechanically contact the surface while has high measurement accuracy and speed, therefore is used in this research. The measurement error happens when the slope of the surface is too large that light cannot be effectively reflected. We will show in Chapter Two that this will cause a great number of fake spikes in both valley and plateau parts of the measure surfaces, which cause the deviation of fiction behavior especially in the dry contact part (caused by fake spikes in plateau part). The numerical generated surface will avoid the fake spikes, and duplicate the friction behavior more accurately compared with the measured surfaces.

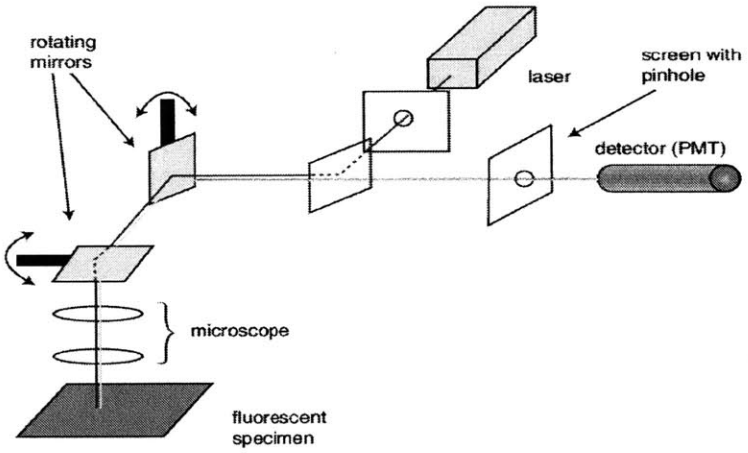

Figure 1. 8: Schematic Drawing of Confocal Microscope [31]

1.4 Wear of Cylinder Liner

The surface geometry of piston liner varies with engine operation time since the solid-to-solid interaction between ring pack and the liner surfaces. In order to manufacture high efficiency and low oil consumption liners, it is important to understand the whole break-in processes.

In Reference 4, a simple method is utilized to simulate the wear process. As Figure 1.9 shown, a grinder line is created by a white noise Gaussian random factor. The line slides with a certain mean height difference above the liner. When the line interacts with the surface, a random proportion is removed from the liner, which follows the uniform distribution between 0 and 1. In each stroke (i.e. one cycle), a new random grinder

surface is generated with the same random parameters. The nominal height h between the grinder line and liner is determined by the following function:

$$\sigma_{combined} = \sqrt{{\sigma_p}^2 + {\sigma_g}^2}$$

$$h = const * \sigma_{combined}$$

Where σ_p and σ_g represent the RMS for plateau of the liner and RMS for the grinder line respectively. Const is usually chosen to be small enough so that there will be interaction between grinder line and liner surface.

Reference 4 shows that if const, σ_g, and cycle are well tuned so that the histogram of numerically generated worn surface matches the specimen, the lubrication behavior will match the experimental data. However, only the new and break-in surfaces (two surfaces) are studied in that research, while the whole worn processes are important and can be used to study the causes of worn, and the parameters affecting the processes. Moreover, the dry contact part is not studied in that research.

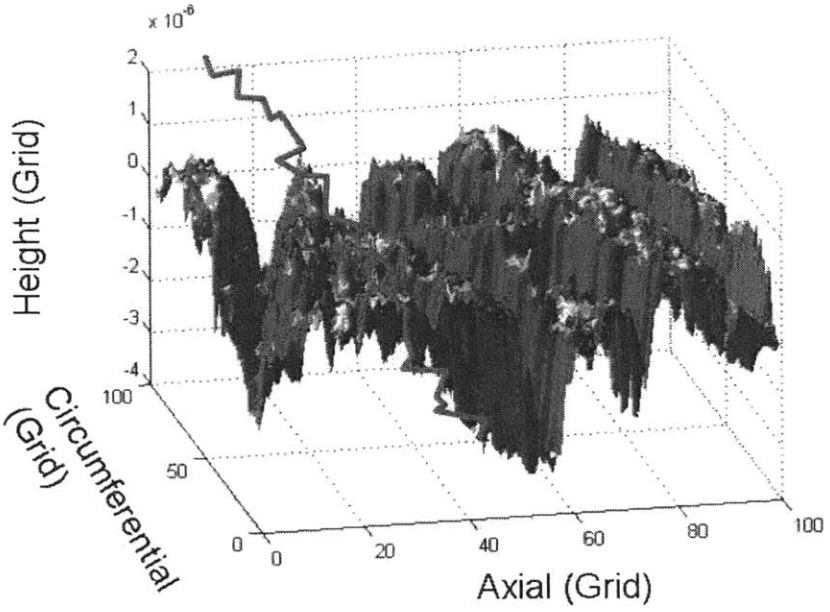

Figure 1. 9: Grinder Line on the Surface Measurement [4]

1.5 Thermal Sprayed Cylinder Liner

Thermal Sprayed cylinder liners are manufactured by the following steps. Before the coating being applied, the bore diameter need to be pre-machined to oversize to

accommodate the coating. Then the liner surface needs to be activated. After the preparation processes, the air plasma spraying (APS) process can be applied to the surface. The coating materials are usually metal matrix composites (MMCs) – a mixture of metal and ceramic. A final coating, the final machining process is applied, which is critical to the geometry (therefore friction behavior) of the liner surfaces. The final honing is carried out by honing the surface with diamond edges. The liner surface has a mirror finish without the plateau part. The optimal sprayed surfaces usually have much smaller RMS compared with honed surfaces [35-38]. Figure 1.10 shows the SEM image of one sprayed surface. The porosity feature of the surface is mainly caused by the spraying process.

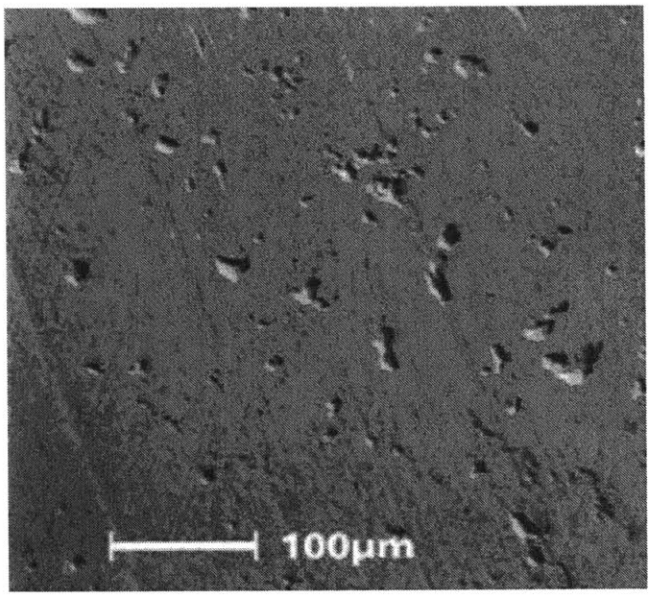

Figure 1. 10: SEM Image of Thermally Sprayed Surface [38]

Experiments shows that compared with honing liner finish, the thermal sprayed liners have couple of advantages. First, the plasma coating of cylinder bores on aluminum cast alloy engine block is lighter compared with the conventional method of using cast iron liner in the aluminum casting. Second, the friction loss decreases. After proper optimization, the potential friction reduction is more than 30 percent. Moreover, the oil consumption also decreases compared with cast iron. Last but not least, the wear resistance of plasma sprayed coating is much higher compared with cast iron [38, 39].

The current researches are mainly based on experiments. In fact, there are plenty of tribology parameters can be optimized to achieve less friction losses and less oil consumption. The numerical methods will save great amount of time. Moreover,

current researches show that the pores in the surface mainly contribute to better lubrication behavior, but the reasons are not convincing. Numerical methods can be developed to study the importance of various geometric parameters of liner surfaces.

1.6 Scope of Thesis Work

The objective of this thesis is to numerically generate liner finish in various conditions, including plateau-honing liners, worn processes, and plasma sprayed surfaces. Moreover, the quantitative relations between different ISO standards for honed surfaces are created. Various tribology parameters of generated liner surfaces are changed and then put into lubrication and dry contact deterministic models. The deterministic parameters are used in engine cycle model, which is used to study the fiction and oil consumption behaviors of engines. The results of the surfaces for deterministic and cycle models are compared, so that we functions of different tribology parameters can be studied.

The second chapter describes the honed liner surface analyzing, generating, testing, and comparing methods. First of all, the method to analyze the topology parameters of honed surfaces (especially the autocorrelation lengths) is described. Second, the honed surfaces are numerically generated and compared with experimental data. Moreover, the topology variables are changed and the corresponding friction behaviors are studied. The relations between topology variables and friction losses are illustrated. Last but not least, we introduce a quantitative relation between ISO 13565-2 standard and ISO 13565-3 standard under normal height distribution for both plateau and valley parts. The former one is usually used in manufacturing industry, while the latter one is used as input for surface generation algorithms. With the quantitative relation, people can easily study and optimize honed surfaces for industry use.

The third chapter tries to simulate the break-in processes for honed liner finish. Not only the start and end states, but also the whole processes are simulated. The friction and pressure behaviors for lightly and heavily worn surfaces are compared with experimental data. Moreover, attempts are made to tune the worn parameters so that the friction effective mean pressure (FMEP) curve can match the experimental data.

The fourth chapter describes the algorithm to numerically generate thermal sprayed liner finish. The hydrodynamic and dry contact friction behavior for generated surfaces are compared with experimental data. Couple of topology parameters are tuned and

their effects on friction losses are studied. Moreover, the effects of the pores created by the plasma spraying processes on the lubrication behavior are simulated.

The fifth chapter concludes the thesis work and describes a few future potential work.

2. Honed Liner Generating

In this chapter, we will describe the honed liner surface analyzing, generating, testing, and comparing methods. First of all, we will introduce the method to analyze the topology parameters of honed surfaces (especially the autocorrelation lengths). Second, the honed surfaces are numerically generated and compared with experimental data. The last but not the least, the topology variables are changed and the corresponding friction behaviors are studied. The relations between topology variables and friction losses are described.

2.1 Analyze Measured Liner Finish

As mentioned in chapter one, confocal microscope has high measurement efficiency, high accuracy, and no mechanically contact the surface during measuring, therefore it is broadly used in industry. All the liner finishes in this thesis are measured by the confocal methods. Figure 2.1 shows the sample surfaces we will use to analyze the topology parameters.

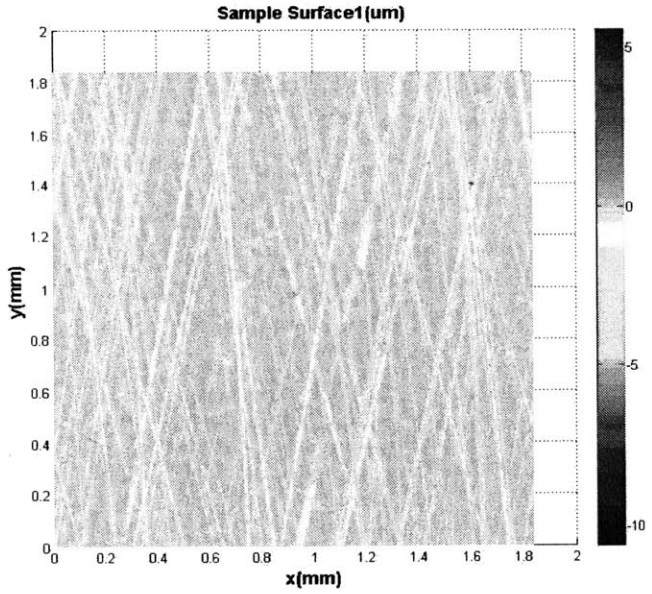

Figure 2. 1: Measured Sample Surface 1 by Confocal Microscope

In order to numerically generate the honed surfaces respecting the physical behaviors of the real surfaces, we need to first calculate the critical topological parameters of the measured surface, and use them as the input for the surface generation algorithm. The parameters we need include RMS for plateau and valley parts, plateau ratio, honing angles, autocorrelation lengths in the orthogonal directions for both plateau and valley.

2.1.1 Calculate Plateau Ratio and RMS for Plateau and Valley

The RMS for plateau and valley parts, and plateau ratio can be obtained by using two straight lines to fit the scaled material ratio curve (i.e. ISO 13565-3 standard mentioned in Chapter One). As Figure 2.2 shown, the slope of blue line represents the RMS for plateau part, and the slope of the green line represents the RMS for the valley part. The intersect point between the green and blue line can be regarded as the interface between plateau and valley. Assuming points above the height is plateau, the value of plateau ratio can be calculated. The red dash line is also the fitted line for the plateau part with different fitting parameters from the blue line. Therefore, there will be calculation difference if one uses different fitting parameters.

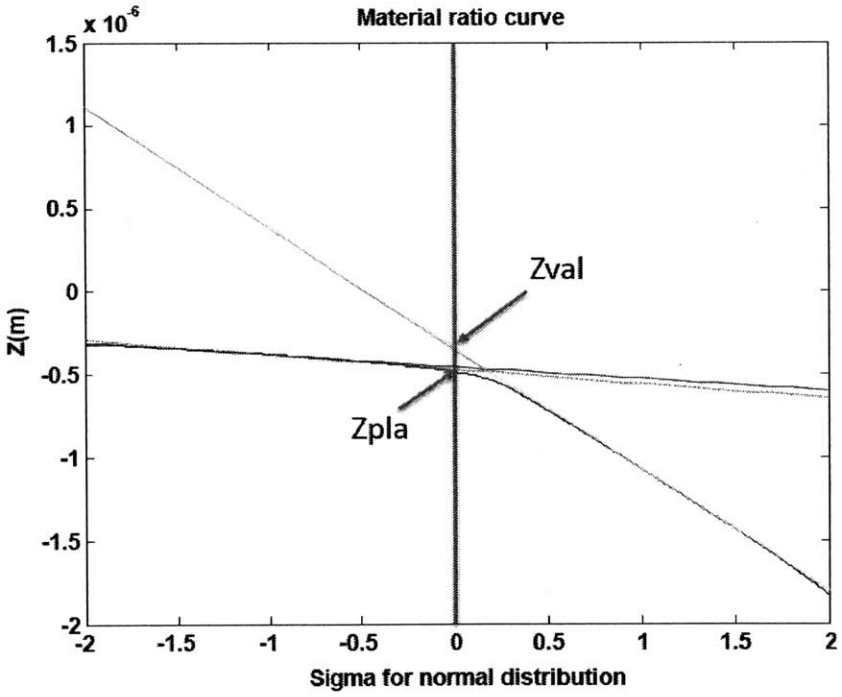

Figure 2. 2: Scaled Material Ratio Curve of Liner Sample1

2.1.2 Calculate Honing Angles and Autocorrelation Lengths

Besides the topology parameters described in ISO 13565-3, we still needs the autocorrelation lengths in orthogonal directions for both valley and plateau parts. In order to calculate the parameters from a measured surface, we need to first separate the plateau and valley part. Therefore we first do fast Fourier Transform and achieve the surface profile in the frequency domain as figure 2.3 shown [11-13]. The line-like patterns correspond to the deep grooves (valley parts) in spatial domain. Each line corresponds to the grooves orthogonal to it. The light cloud-like patterns correspond to the valley part, which are isotropic. They can be regarded as the background. Therefore, the next task is to extract the line patterns from the cloud pattern background.

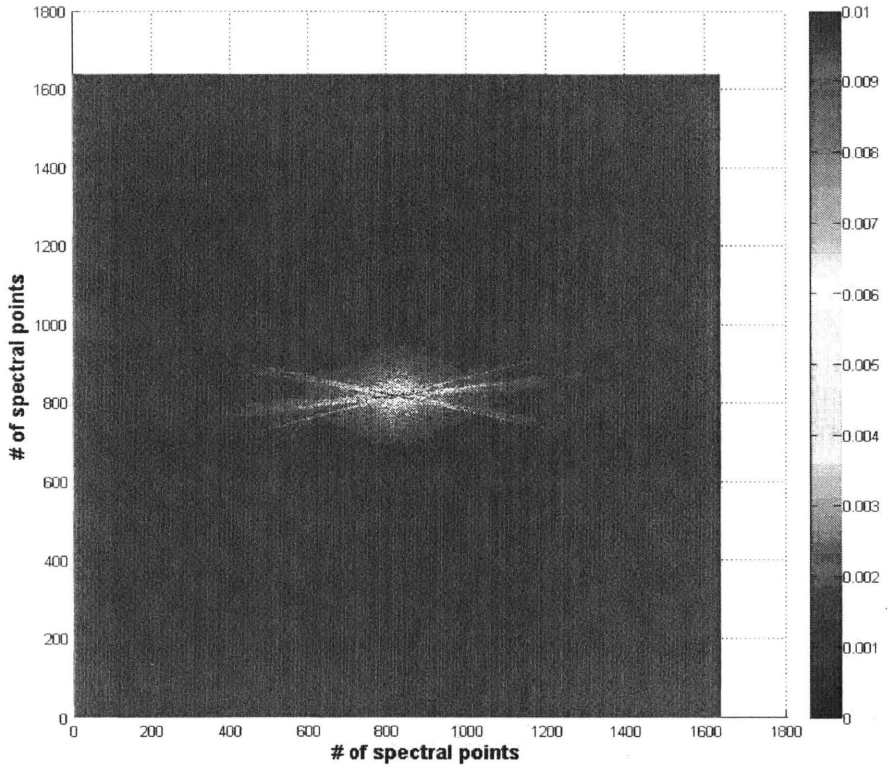

Figure 2. 3: Liner Finish Sample1 in Frequency Domain (scaled intensity)

Next the frequency domain is transformed to the polar coordinate. The spectral power is integrated at each angle. Figure 2.4 shows the power distribution. The peaks correspond to the angles of the line patterns, but some fake ones appear since it is

difficult to identify the angles of low frequency components (near the center). Additionally, the boundary effect caused by FFT also leads to fake peaks (e.g. the peak at angle of 90). Therefore, in order to identify the angle of line patterns, we need to pay attention on the high frequency components, and low pass filter is applied. Fig. 2.5 shows the spectral power distribution after filtering. The peaks are more obvious compared to the former one, and fake ones are suppressed.

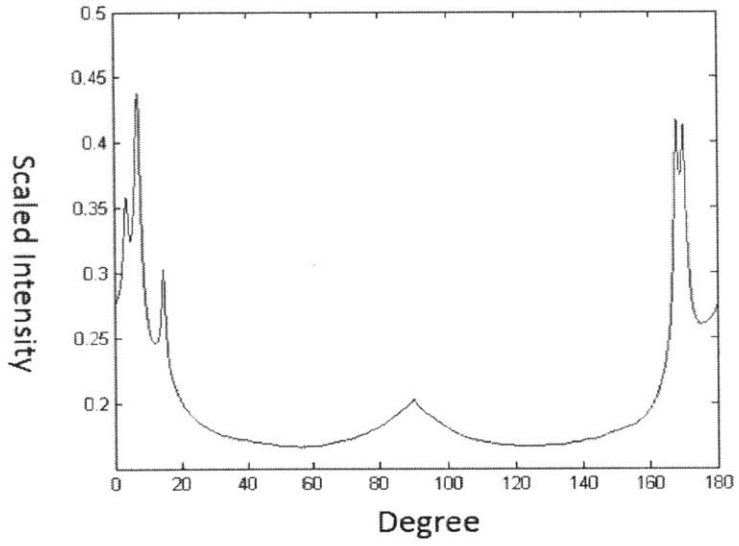

Figure 2. 4: Original Spectral Power Distribution in Polar Coordinates

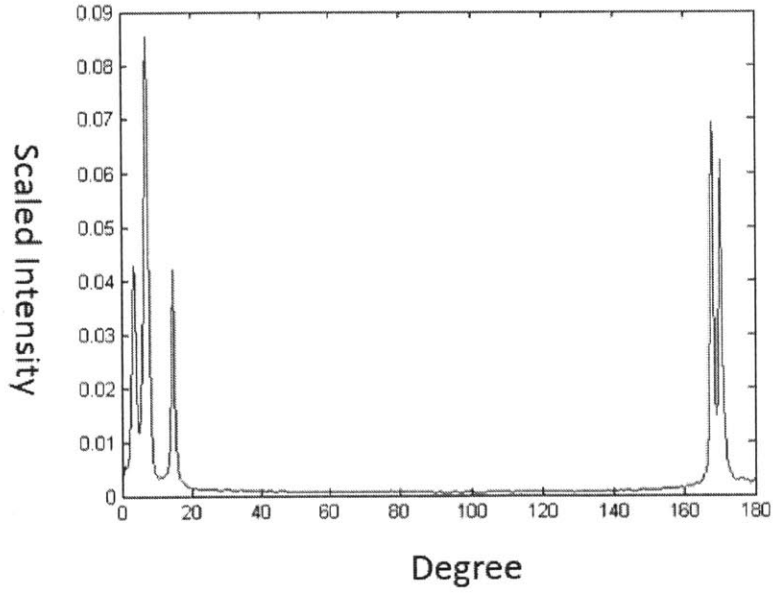

Figure 2. 5: Spectral power distribution in polar coordinates after low-pass filtering

Based on the spectral power distribution, line patterns and its corresponding honing angles and energy intensity can be effectively extracted from the cloud pattern background. The energy intensity is linearly related to the square of RMS for each part. Therefore, based on the energy intensity of each part and the total RMS for plateau and valley, the RMS for each part can be calculated. Then inverse FFT is respectively applied to the cloud patterns and line patterns in each direction. The inverse FFT of the cloud patterns correspond to the plateau parts in the original surface (as Figure 2.6 shown). Compared to the original surface, it is easy to find that the deep grooves have been depressed in Figure 2.6, indicating good separation. Figure 2.7 represents the inverse FFT of one of the line patterns. They are the deep grooves in the direction orthogonal to the line pattern.

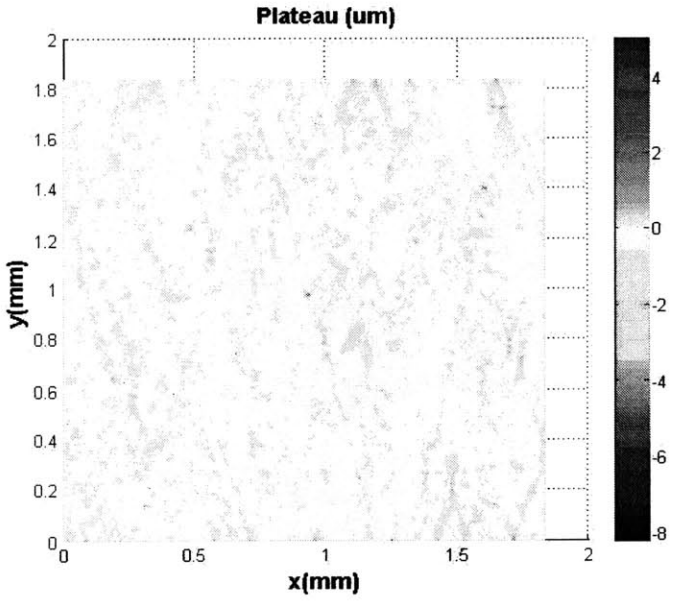

Figure 2. 6: Inverse FFT of the Cloud Patter (Plateau Part)

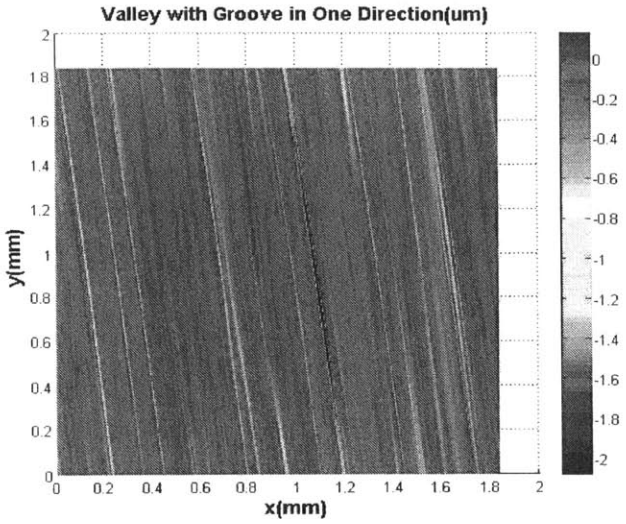

Figure 2. 7: Inverse FFT of the Line Pattern in One Direction (Groove in Valley)

After separating the plateau and valley parts, the autocorrelation function (ACF) and autocorrelation lengths are calculated for each part. ACF can be achieved by conducting the inverse FFT of the spectral power. Autocorrelation length corresponds to the distance where ACF drops to 10% from its largest value (As mentioned in Chapter One).

2.1.3 Honed Surface Generation Processes

Once we achieve all the parameters from the measured surface, we are able to numerically generate a surface using the method described in Chapter One. In order to confirm the accuracy of the generating algorithm, the generated surface should have the same physical behavior (pressure, friction, and oil consumption) as the original surface.

First of all, we will generate the valley part with groove in each direction as Figure 2.8 shown. Then we combine the valley parts according to the honing angles achieved from the FFT of the measured surface as Figure 2.9 left shown. Similarly, the plateau part can be generated. Finally, the plateau and valley parts are combined according to the plateau ratio. The final generated surface is shown in Figure 2.10.

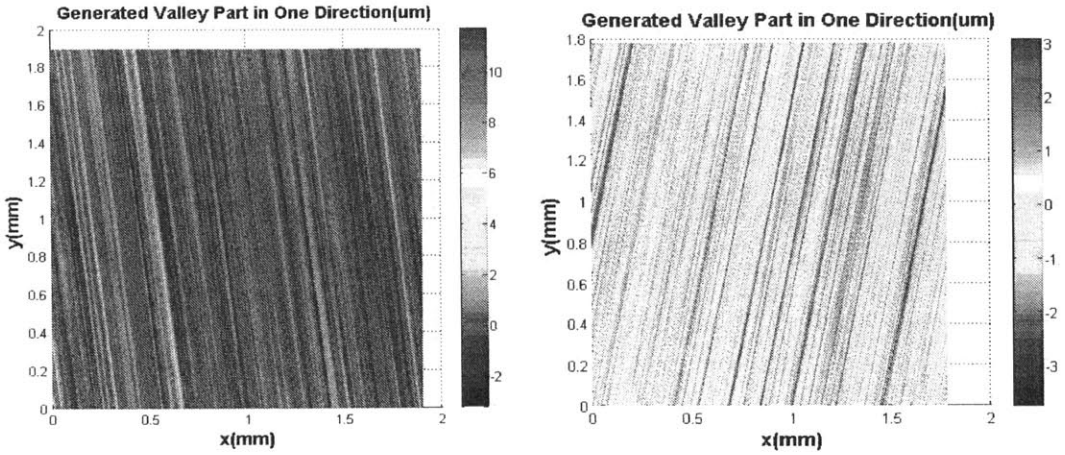

Figure 2. 8: Generated Valley Part in Each Direction

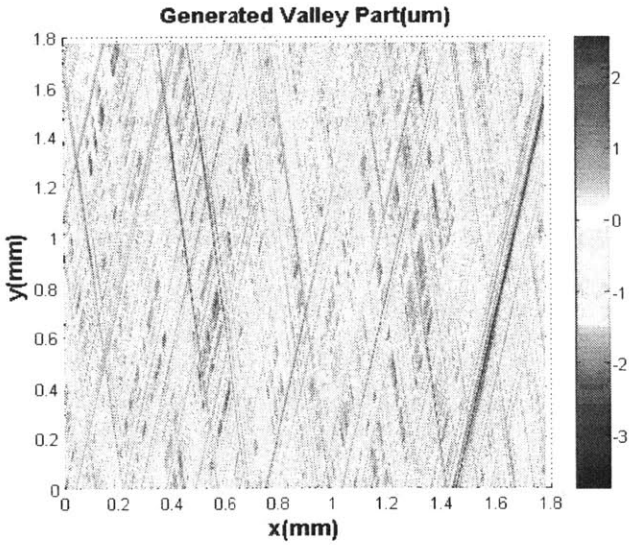

Figure 2. 9: Generated Valley Part

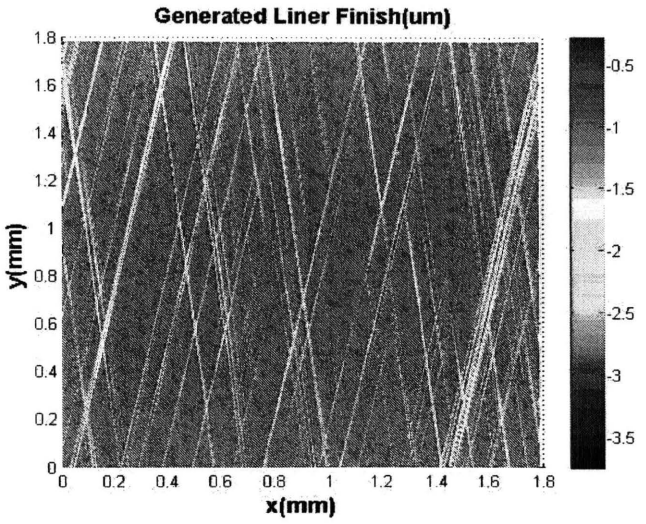

Figure 2. 10: Generated Honed Liner Finish

Figure 2.11 concludes the processes of calculating the topological parameters of the surface, and Figure 2.12 concludes the processes of numerically generating honed surfaces.

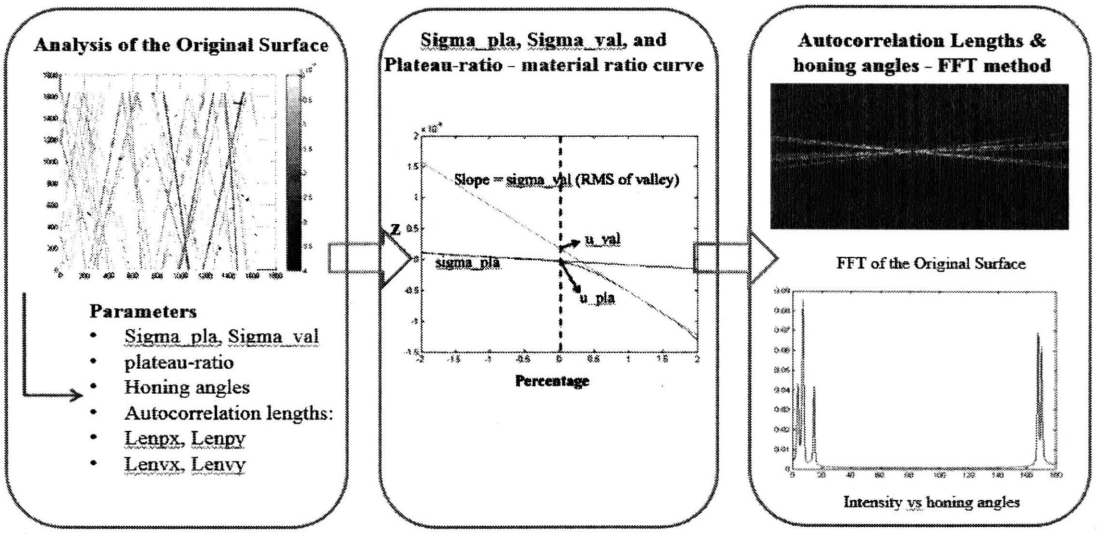

Figure 2. 11: Processes of Calculating Topological Parameters of Measured Surfaces

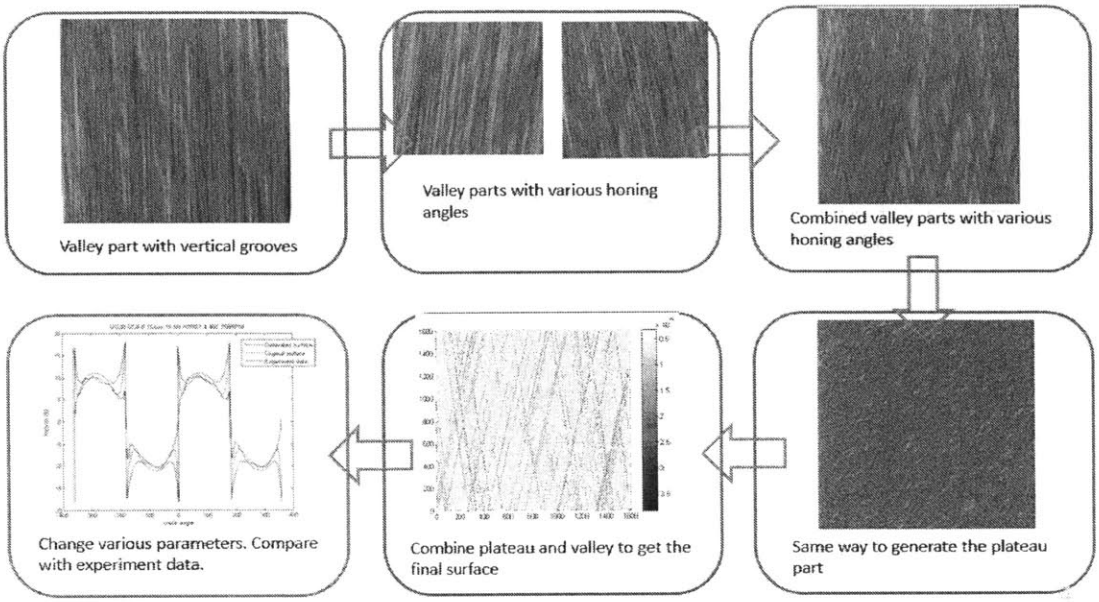

Figure 2. 12: Processes of Numerically Generating Honed Liner Finishes

2.2 Test of Liner Finish Generation Method

In order to compare the friction behavior of generated surface, measured surface, and experimental data, we first use each surface in the hydrodynamic deterministic model [4-6]. Figure 2.13 shows the histogram comparison between measured and generated surfaces. It shows that the RMS for the generated plateau part is larger compared with the measured one, which is caused by the calculation error due to fake spikes in the measure surface.

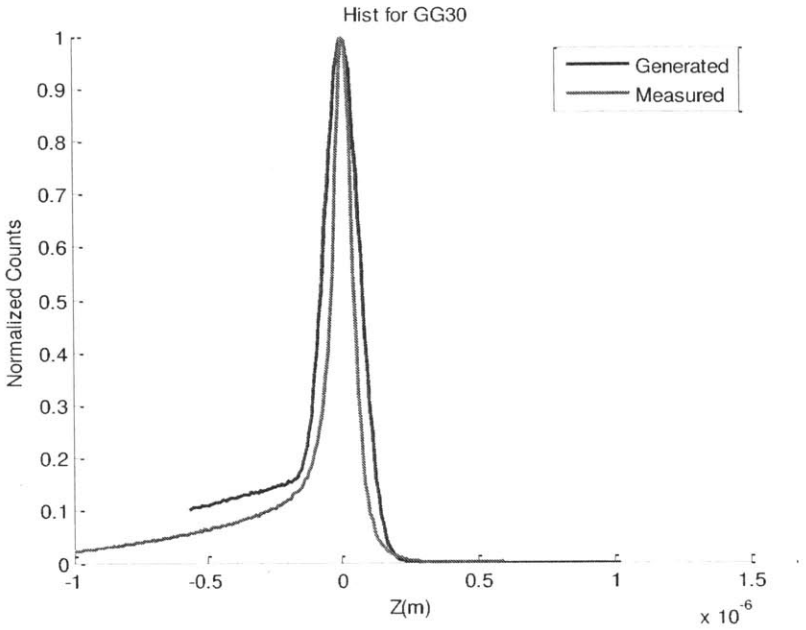

Figure 2. 13: Histogram Comparison of Liner Finish Sample 1

Figure 2.14 shows the hydrodynamic pressure and friction curve in each normalized height for the generated and measured surface. The red line represents the generated surface, while the blue line represents the measured surface. From the figures, we find that the generated surface has the similar lubrication behavior as the measured surface.

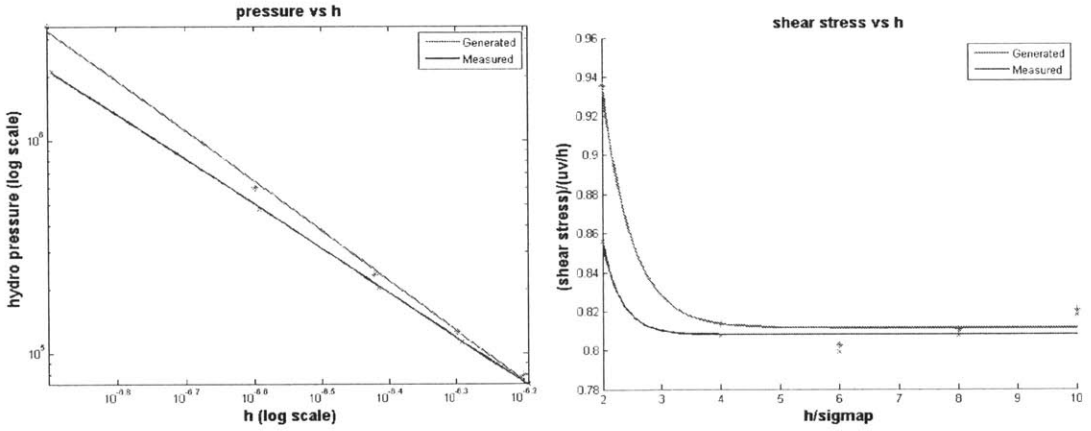

Figure 2. 14: Hydrodynamic Pressure and Shear Stress Curve for Liner Sample1

Similarly, the generated and measure surfaces are put into the dry contact determinist model which is developed by Lubrecht [40]. Figure 2.15 shows the dry load in each

normalized height. There are obvious difference between the generated surface and the measured one.

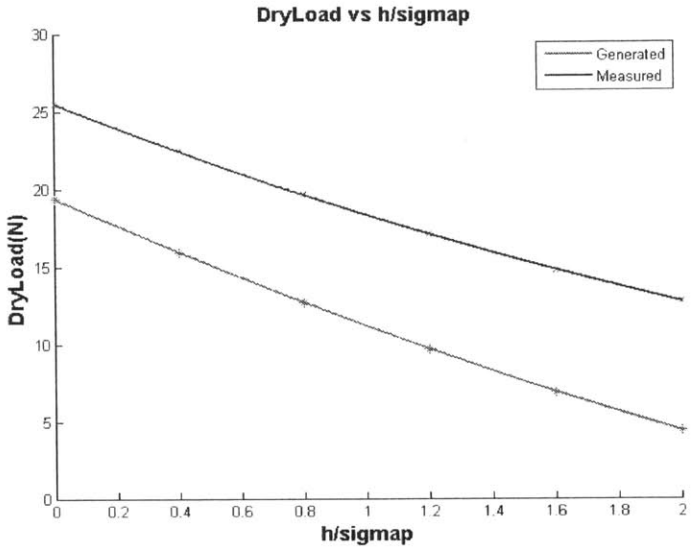

Figure 2. 15: Dry Load Curve for Liner Sample1

In order to find out the reasons for the difference in the dry contact load, the engine cycle model is used so that both the generated surface and measure one can be compared with experimental data. The parameters from determinist models are used as input.

Figure 2.16 shows the friction curve under one complete cycle when the temperature is 40C and the rotation speed is 700 revolutions per minute (RPM). The blue line is the experimental data [41]. The shape of the curve shows that it is hydrodynamic dominated. The red dash line is the measured surface, which deviates a lot compared with the experimental data. We use the hydrodynamic parameters from measured surface and the dry contact parameters from generated surface as inputs to achieve the red solid line. This line matches well with the experimental data, indicating that the major deviation is from the dry contact part, namely the plateau part of the measured surface. The black line represents the generated surface, which also matches well with the experimental data, indicating the surface generation method is reliable.

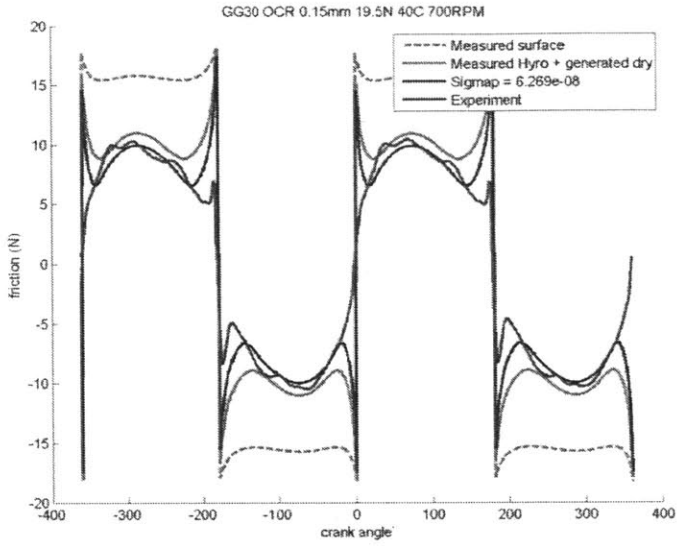

Figure 2. 16: Sample 1 Cycle Model Comparison under 40C and 700 RPM (Lubrication Dominated)

Figure 2.17 shows the friction curve when temperature is 100C and the rotation speed is 500 RPM. The blue line represents the experimental data, which reflects that the friction is a mixture of both lubrication and dry contact parts. The red dash line represents the measured surface, which deviates a lot compared with the experimental data. The black line is the generated surface according to the measured surface, which matches the experimental data better compared with the measured surface but still deviates. If we generate surface with smaller RMS for plateau (sigmap = 3.127e-08 m), the friction curve matches well. Therefore, the major reason for deviation of the generated surface is that the calculated sigmag based on the measured surface is larger than the real value.

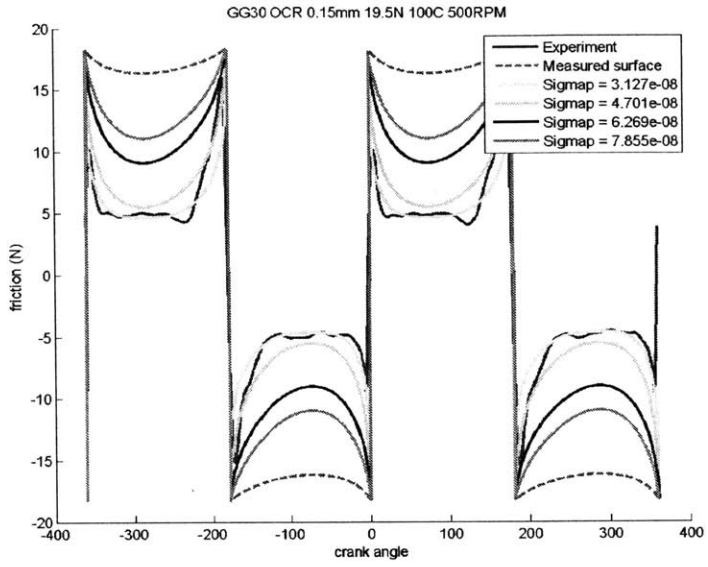

Figure 2. 17: Sample 1 Cycle Model Comparison under 100C and 500 RPM (Dry Contact Exists)

In conclusion, the generated surface matches the experimental data well in the lubrication part (even better than the measured surface), while it has deviation in the dry contact part (but still better than the measured surface). The major reason is the great number of fake spikes in the measured surface caused by the measurement error of the confocal microscopy described in Chapter One. Figure 2.18 shows the 3D roughness data of sample 1 liner finish. The light blue spots represent the fake spikes. They not only increase the dry contact pressure in the deterministic model, but also increase the RMS for plateau. The generated surface is generated based on normal distribution assumption, therefore does not have fake spikes and matches the experimental data better compared with the measured surface.

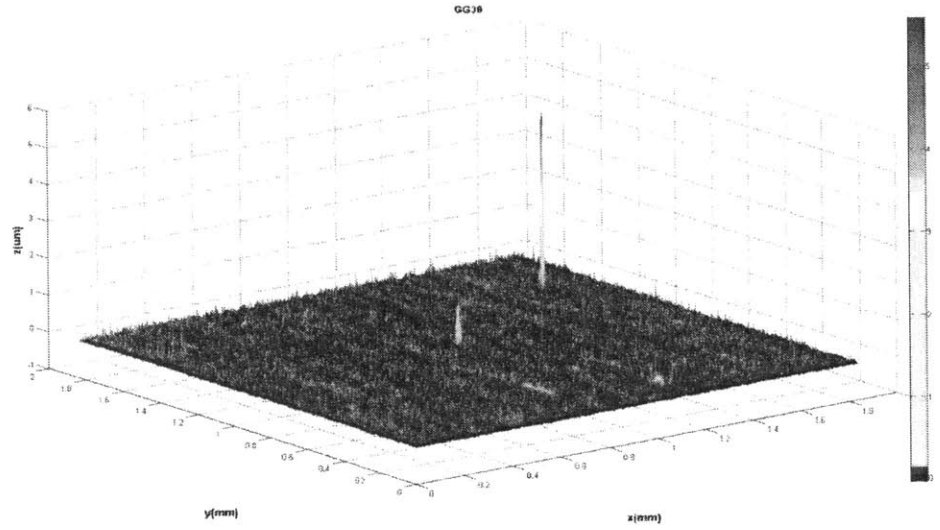

Figure 2. 18: Roughness Data of the Sample 1 Liner Finish (um)

In order to double check the reliability of the algorithm, liner finish sample 2 is analyzed and generated. As Figure 2.19 shown, the topology of sample 2 is quite different from sample 1. Quantitatively, for sample 1, the RMS for valley and plateau are 6.9670e-07m and 6.2501e-08m. In contrast, for sample 2, the RMS for valley and plateau are 1.7839e-07m and 7.1544e-08m, which are much smaller (especially the valley part) compared with sample1, implying that the depth of grooves for sample 2 are smaller than that for sample 1. The plateau ratio for sample 1 is 53.24%, while that for sample 2 is 36.19%, indicating that sample 1 has more plateau compared with sample 2. Moreover, for sample 1, the autocorrelation lengths for valley and plateau are 14 and 21.5 (# of measurement points), while those for sample 2 are 5.5 and 11.5, much smaller compared with sample 1. This means that the local micro-structures for sample 1 are larger than sample 2. Figure 2.20 shows the comparison of histograms for sample 1 and sample 2. It is obvious that the height distributions for the two surfaces are also different. All in all, the topology of the two liner finishes are different. If the generated surfaces can well simulate the friction behaviors of both surfaces, the reliability of the surface generating algorithm can be confirmed.

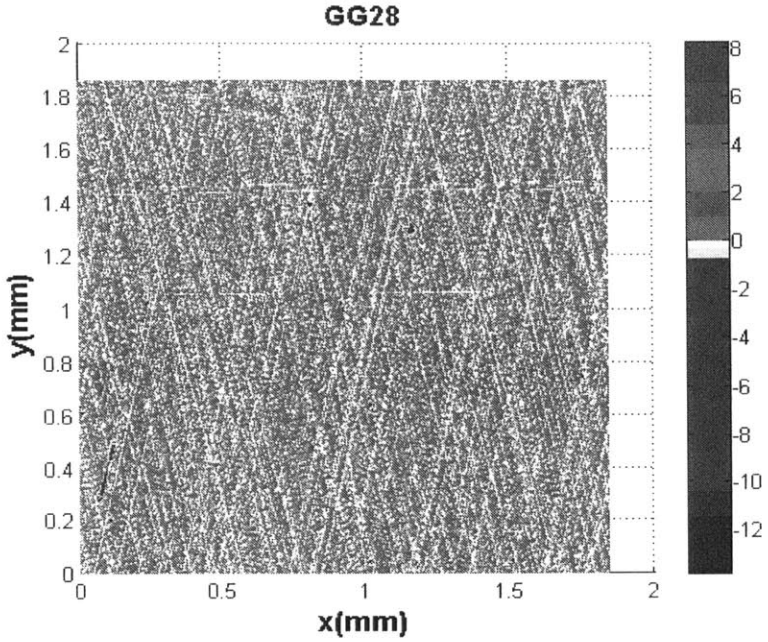

Figure 2. 19: Liner Finish Sample 2 (um)

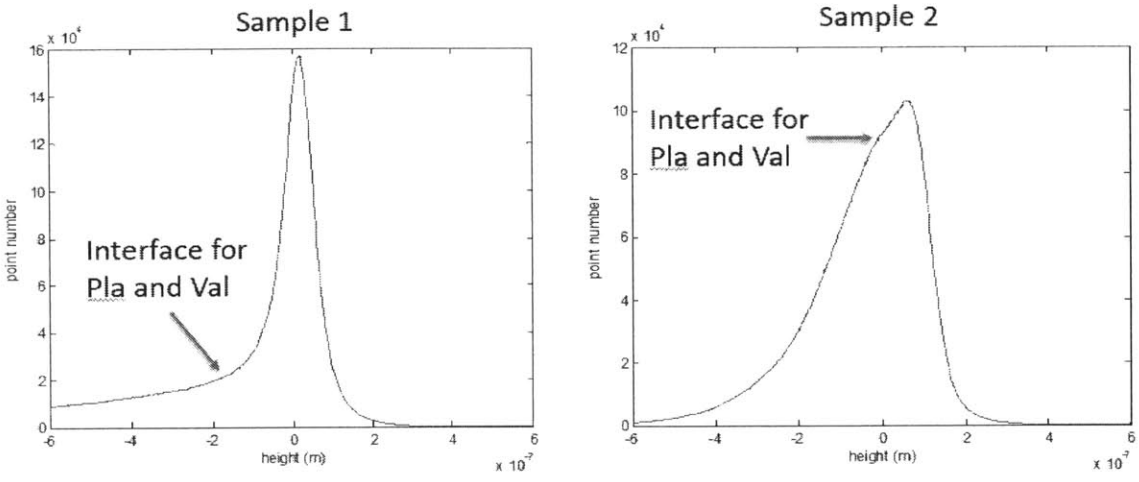

Figure 2. 20: Histogram Comparison for Sample 1 and Sample 2

Figure 2.21 shows the histogram comparison of generated and measured liner finish sample 2. It shows that the majors shapes and intersect position between plateau and valley are similar. The RMS for plateau part should be decreased.

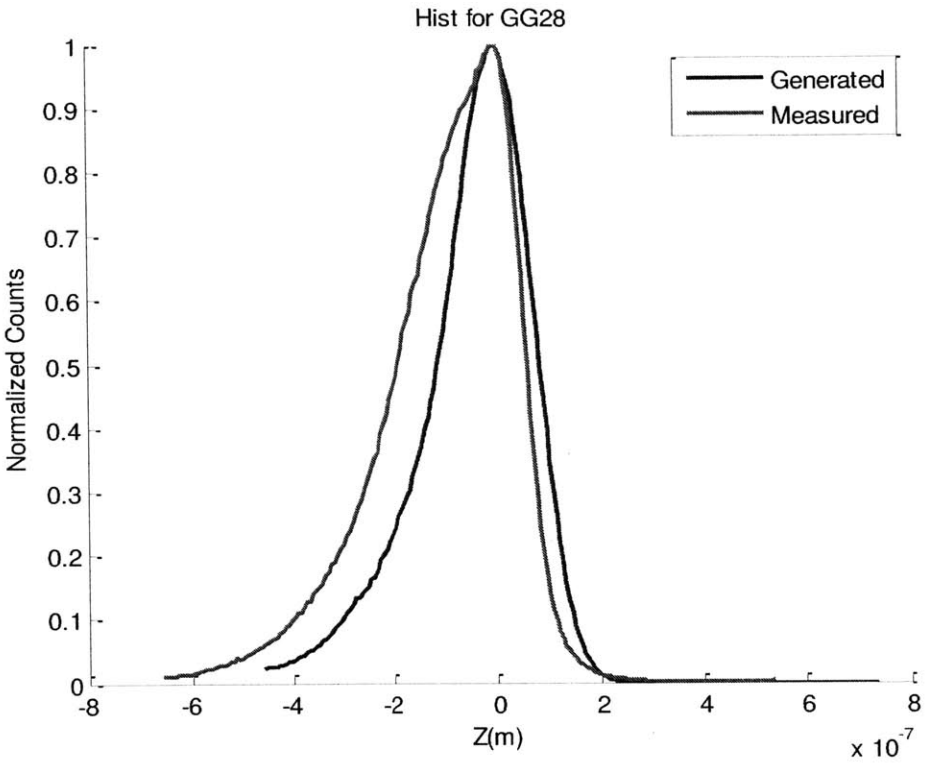

Figure 2. 21: Histogram Comparison of Liner Finish Sample 2

Figure 2.22 shows the hydrodynamic pressure and friction curve in each normalized height for the generated and measured surface based on sample 2. The red line represents the generated surface, while the blue line represents the measured surface. From the figures, we find that the generated surface has larger pressure and friction compared with the measured surface.

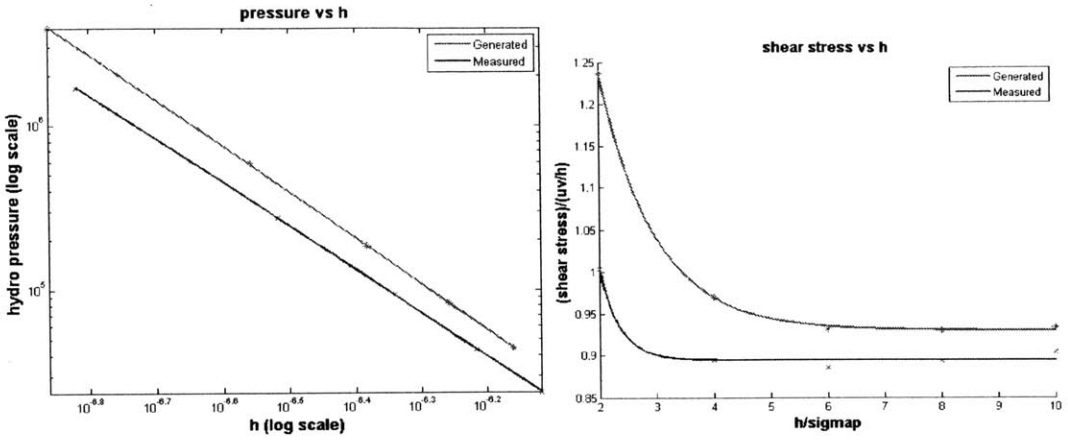

Figure 2. 22: Hydrodynamic Pressure and Shear Stress Curve for Liner Sample2

Similarly, the generated and measure surfaces are put into the dry contact determinist model. Figure 2.23 shows the dry load in each normalized height. The two curves match very well.

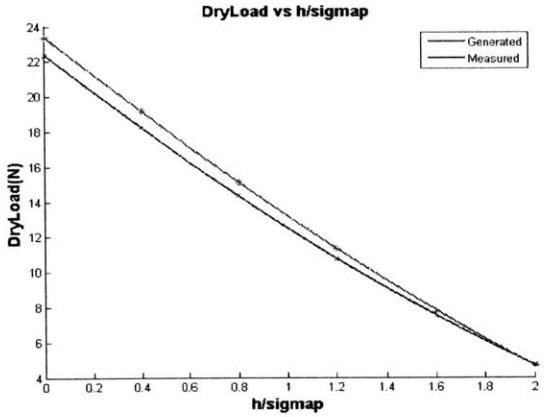

Figure 2. 23: Dry Load Curve for Liner Sample 2

In order to find out the reasons for the difference in the lubrication part, the engine cycle model is used so that both the generated surface and measure one can be compared with experimental data. The parameters from determinist models are used as input.

Figure 2.24 shows the friction curve under one complete cycle when the temperature is 40C and the rotation speed is 700 revolutions per minute (RPM). The blue line is the experimental data. The shape of the curve shows that around the center of each curve, it is hydrodynamic dominated. The red dash line is the measured surface, which

deviates compared with the experimental data. We use the hydrodynamic parameters from measured surface and the dry contact parameters from generated surface as inputs to achieve the red solid line. This line matches with the red dash line, indicating that the dry contact parts difference for sample 2 is smaller compared with sample 1. The black line represents the generated surface, which matches well with the experimental data, indicating the surface generation method is reliable. The major difference between the generated surface and the measured surface is the hydrodynamic part, namely the valley part.

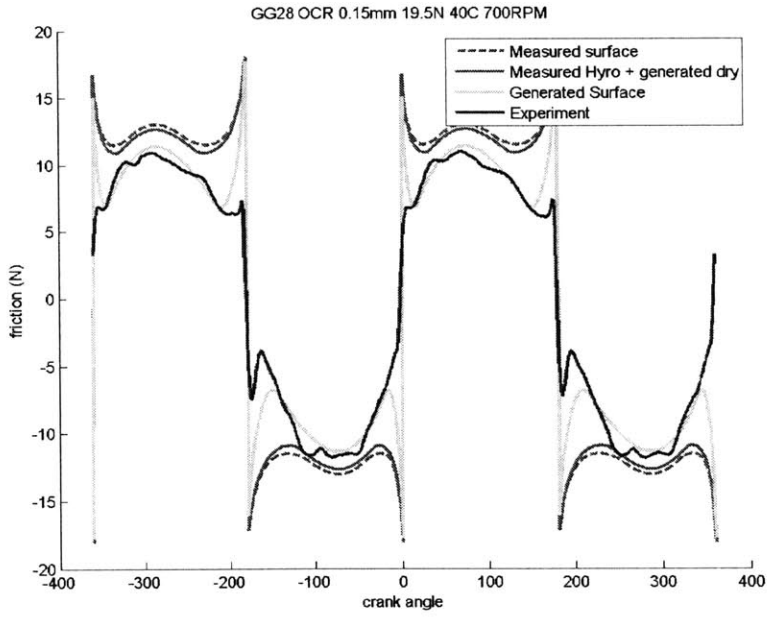

Figure 2. 24: Sample 2 Cycle Model Comparison under 40C and 700 RPM (Lubrication Dominated)

Figure 2.25 shows the friction curve when temperature is 100C and the rotation speed is 500 RPM. The blue line represents the experimental data, which reflects that the friction is a combination of both lubrication and dry contact parts. The red dash line represents the measured surface, which deviates a lot compared with the experimental data. The green line is the generated surface according to the measured surface, which matches the experimental data better compared with the measured surface but still deviates. This means that there are also fake spikes in the plateau part of sample 2.

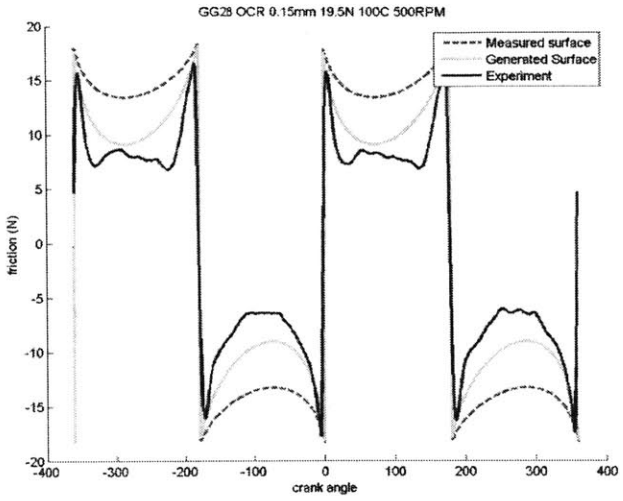

Figure 2. 25: Sample 2 Cycle Model Comparison under 100C and 500 RPM (Dry Contact Exists)

Comparing the cycle model results for liner finish sample 1 and sample 2, we find that for sample 1, the major difference for generated surface and measured surface exists in the dry contact part, which is mainly caused by the great number of fake spikes in the plateau part. In contrast, for sample 2, the difference for the plateau parts is smaller, while the difference for the valley parts is larger, indicating that there are less fake spikes in the plateau part and more fake spikes in the valley part. This can be confirmed by the plateau ratio value – the plateau area for sample 1 is much larger. Figure 2.26 shows the plateau of sample 2, which shows obviously less fake spikes (light blue parts) compared with sample 1.

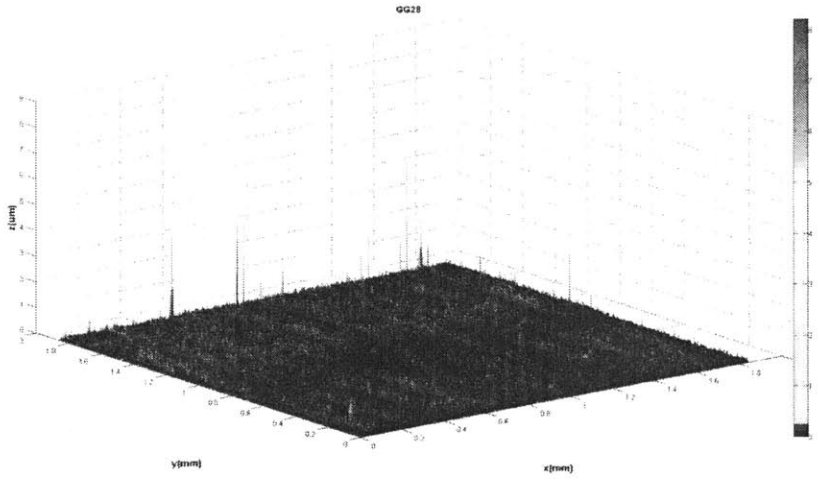

Figure 2. 26: Roughness Data of the Sample 1 Liner Finish (um)

2.3 Study Topology Variables by Surface Generating Algorithm

In this section, we will use the liner finish generating algorithm to generate surfaces with difference values of topology parameters (based on sample 1), and put them into the deterministic models. Therefore, we can find the effects of various topology parameters on the engine operation behavior. For each parameter, the hydrodynamic pressure, friction ratio, friction coefficient, and dry contact pressure curves are plotted, where friction ratio and friction coefficient means:

$$friction\ ratio = \frac{shear\ stress}{\frac{\mu u}{h}}$$

$$\text{friction coef} = \frac{\text{shear stress}}{\text{pressure}}$$

where h is the height difference between the ring and the liner finish, μ is the viscosity, and u is the piston sliding velocity.

First of all, the parameters of the plateau part are studied. The RMS for plateau (sigmap) is changed and other parameters are fixed as figure 2.27 shown. When sigmap increases, the hydrodynamic pressure increases, friction ratio increases, friction coefficient decreases, and dry contact load increases.

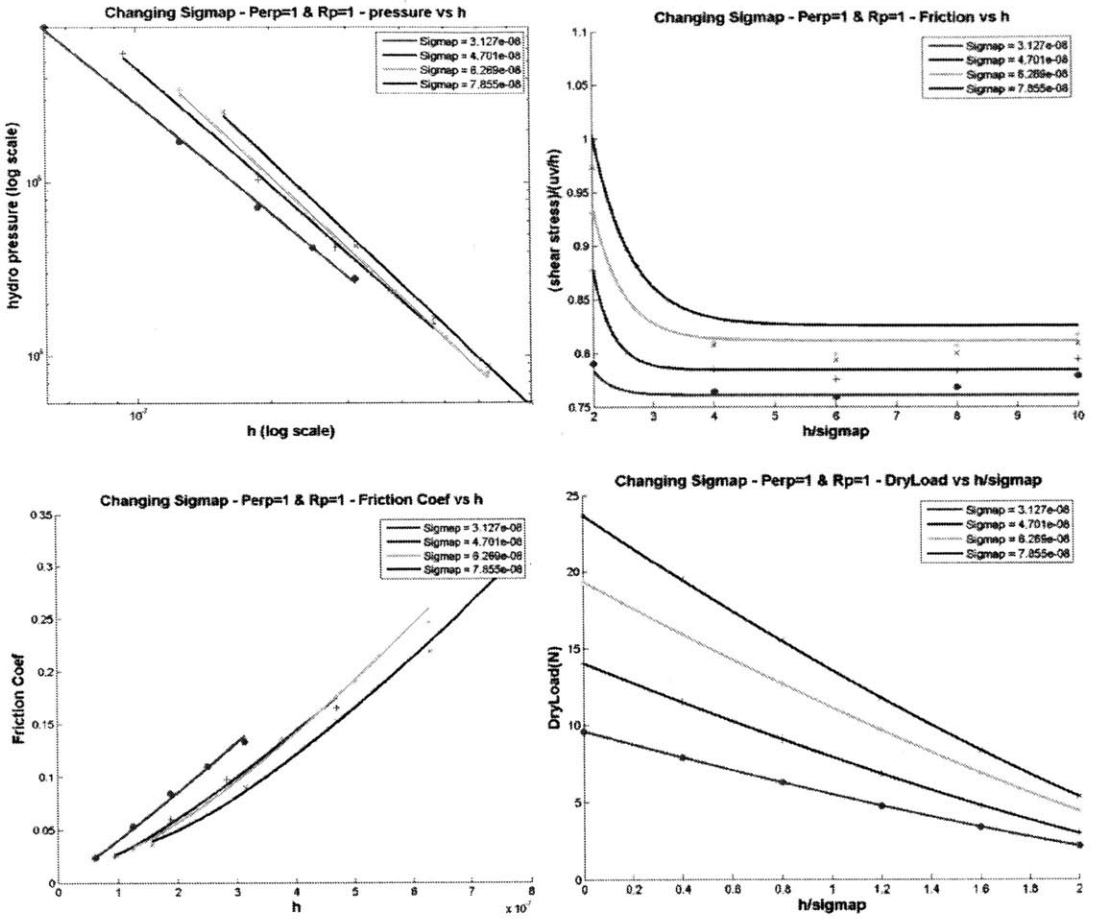

Figure 2. 27: Deterministic Model Curves for Various RMS for Plateau

Besides the analytic relations, the quantitative relation can also be developed. In Greenwood's model using Herzian Theory [8], the relation between sigmap and dry contact load follows the equation:

$$p_c = \frac{8\sqrt{2}}{15}\pi N\beta\sigma_p E'\sqrt{\frac{\sigma_p}{\beta}}F_{\frac{5}{2}}\left(\frac{h}{\sigma_p}\right)$$
$$= C * \sigma^{1.5} * F_{\frac{5}{2}}\left(\frac{h}{\sigma_p}\right)$$

Which means that the pressure dependency on $sigma_p$ should be power of 1.5. The deterministic model is a more accurate in physics as it considers the effect of the contact pressure on the deformation of the entire surface, which is not considered in the Greenwood's model. However, the quantitative relation between $sigma_p$ and dry

contact load is unclear in the deterministic model. Using the surface generating method and the dry contact curve above, Figure 2.28 is plotted. Each dry contact load is divided by the smallest dry contact. In the right figure, sigmap (x axis) is also divided by the smallest value. Since the points in the left figure follows three parallel lines, there is a fixed relation between dry contact load and sigmap. The right figure shows the points can be fitted by a straight line, therefore the dry contact pressure dependency on sigmap is power of 1 for deterministic model.

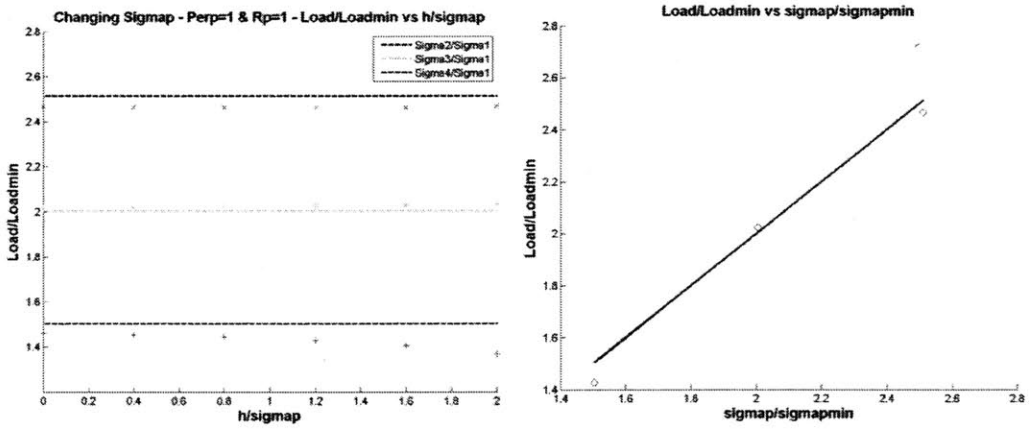

Figure 2. 28: Scaled Dry Contact Load Curve to Scaled Height

Figure 2.29 shows the cycle model results for different values of sigmap. The top figure shows ¼ cycle under 40 degree and 700 RPM. The shape shows that around the center it is hydrodynamic dominated. The change of sigmap does not have significant effects on the hydrodynamic behavior, which matches the fact that hydrodynamic behaviors are mainly controlled by the valley part. The bottom figure shows the pressure curve under 100 degree and 500 RPM. The shape of the curve shows that it is a combination of hydrodynamic and dry contact effects. Larger value of sigmap leads to larger friction, which fits the fact that rougher plateau will cause larger dry contact pressure.

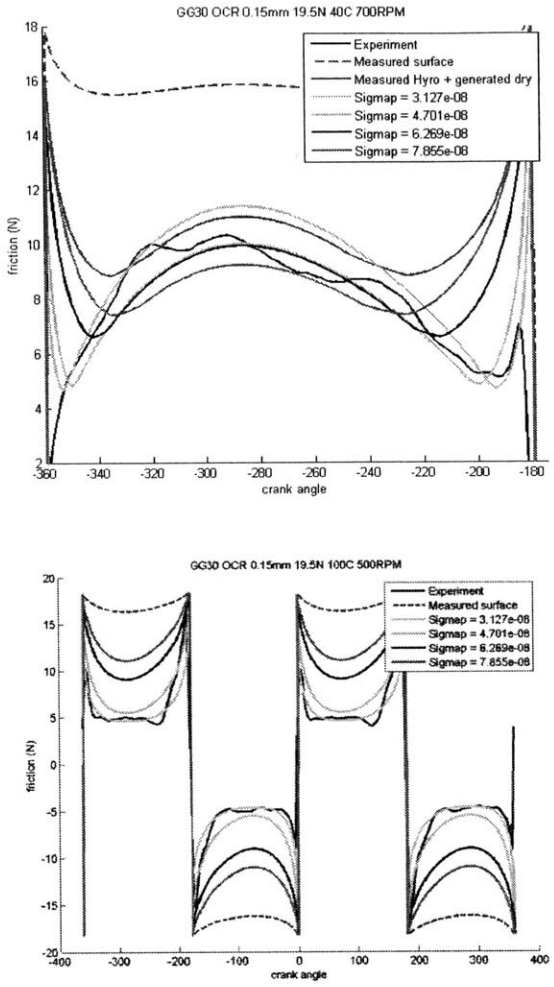

Figure 2. 29: Cycle Model Results for Various Values of Sigmap

Next, the values of autocorrelation lengths for plateau part are changed. Autocorrelation lengths are directly related to local structure shapes. Larger autocorrelation length means larger local microstructures on the liner finish. Figure 2.30 shows the results from deterministic models. Autocorrelation lengths do not have obvious effects on deterministic parameters (neither hydrodynamic nor dry contact). For Greenwood's model using Hertian theory, the dry contact pressure has the following equation [8]:

$$p_c = \frac{8\sqrt{2}}{15}\pi N\beta\sigma_p E'\sqrt{\frac{\sigma_p}{\beta}}F_{\frac{5}{2}}\left(\frac{h}{\sigma_p}\right)$$

Where β relates to autocorrelation length for plateau. From the relation, it is obvious that pressure should be related to $\beta^{-0.5}$, while from the fourth figure of Figure 2.30, for the deterministic model it shows that the dry contact pressure is almost independent on autocorrelation length of plateau part.

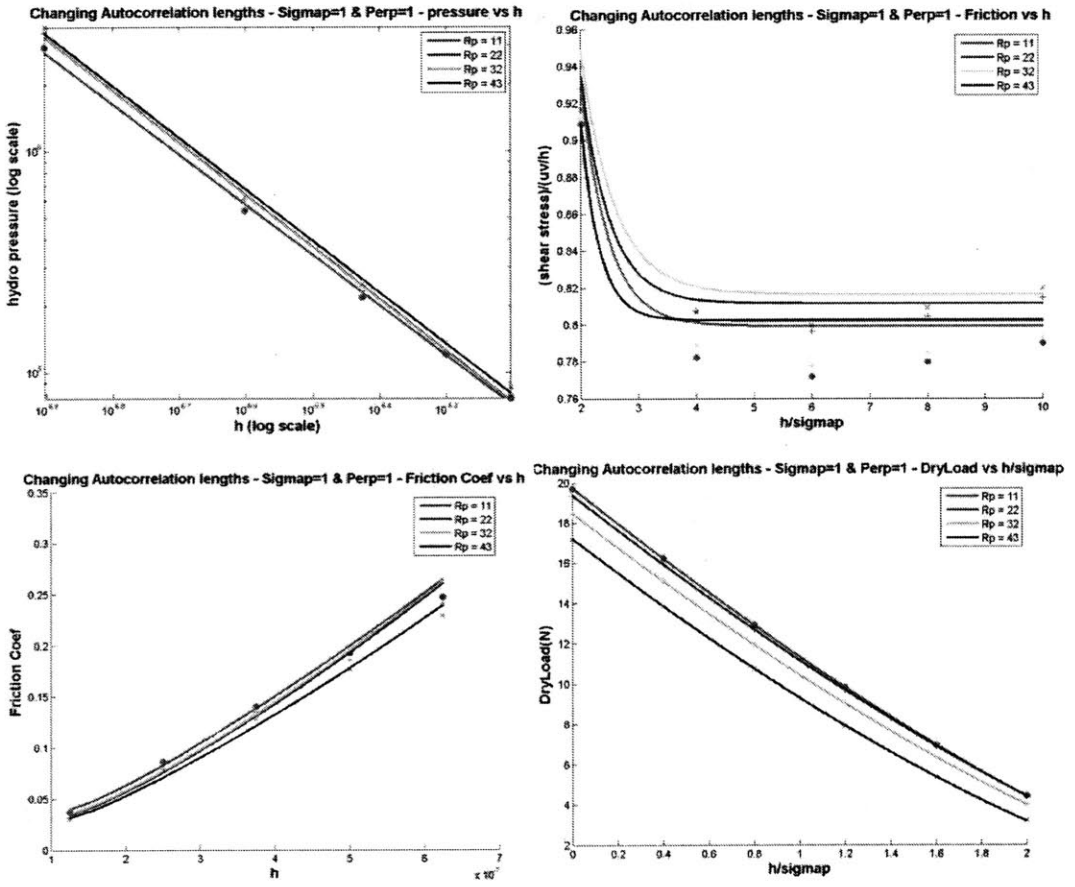

Figure 2. 30: Deterministic Model Curves for Various Values of Autocorrelation Lengths for Plateau Part

Next the values of plateau ratio is changed. Figure 2.31 shows the deterministic model curves. When plateau ratio increases, the hydrodynamic pressure and friction ratio increases, while the friction coefficient almost remains the same. When plateau ratio increases, the dry contact load also increases since the area of plateau increases.

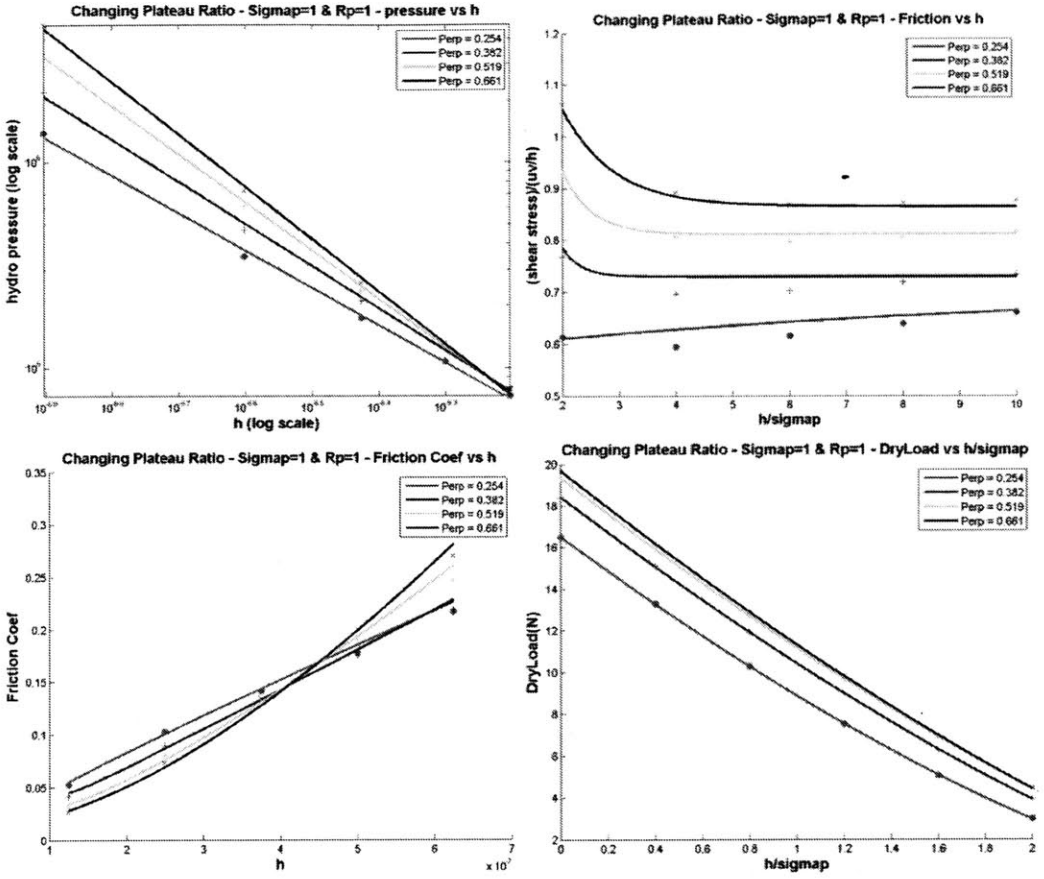

Figure 2. 31: Deterministic Model Curves for Various Values of Plateau Ratio

Next, the topology parameters in the valley part are studied. First of all, the RMS of valley part (sigmav) is studied. Figure 2.32 shows the deterministic model curves. Larger value of sigmav causes lower hydrodynamic pressure, lower hydrodynamic friction, and higher friction coefficient. Larger value of sigmav also causes lower dry contact load.

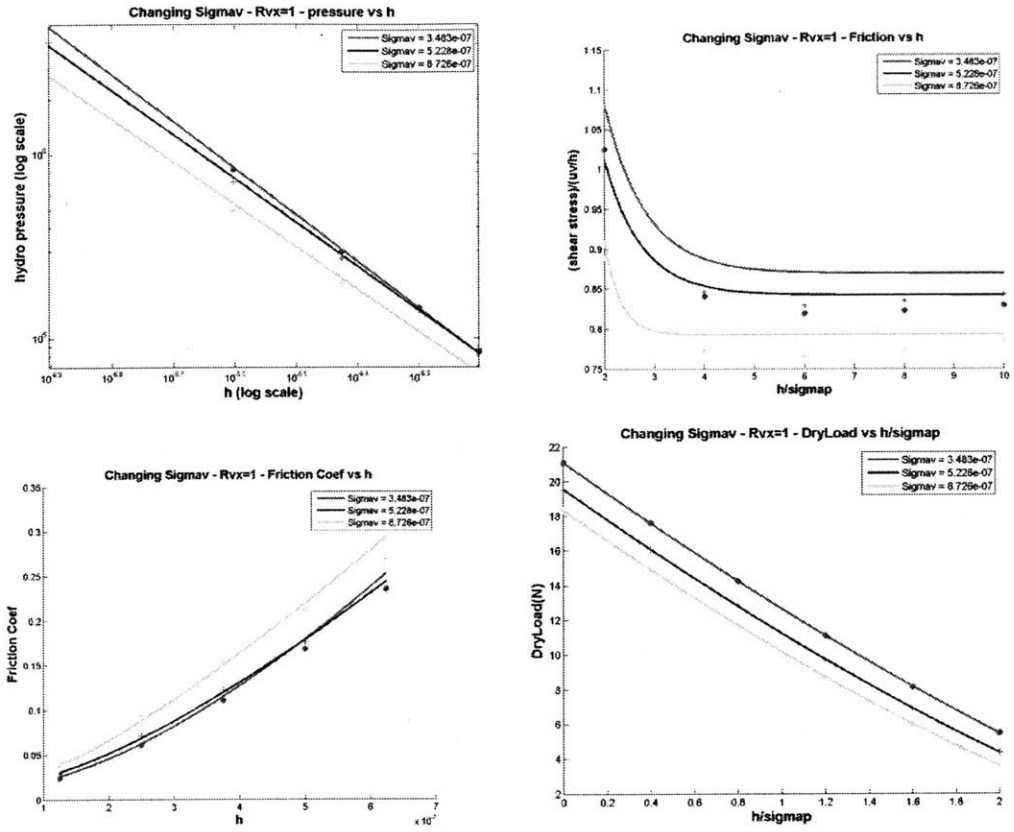

Figure 2. 32: Deterministic Model Curves for Various Values of RMS for Valley Parts

Next, the autocorrelation length vertical to the grooves of valley part is studied. The larger value of the autocorrelation length leads to wider groove. Figure 2.33 shows the deterministic model curves. When autocorrelation length increases, the hydrodynamic pressure increases at first, and then stay the same since the autocorrelation lengths (groove width) approaches the ring land width. The hydrodynamic friction and dry contact load are not apparently affected by the change of autocorrelation value. The friction coefficient decreases as the autocorrelation length increases.

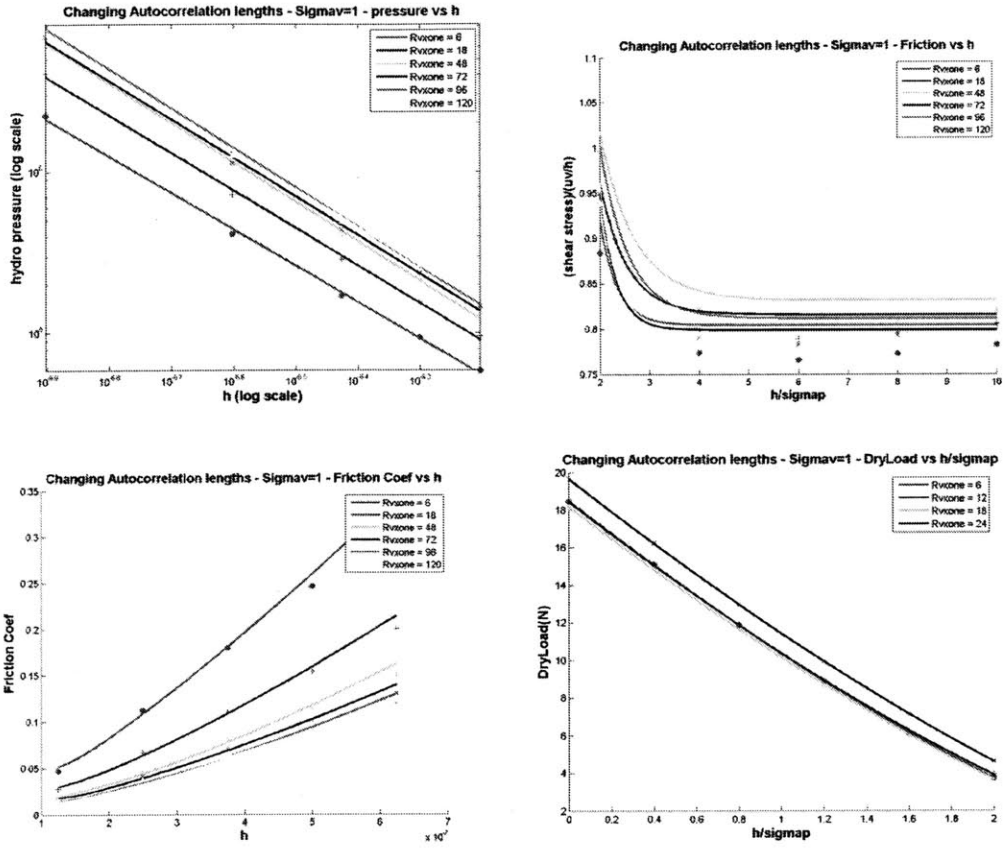

Figure 2. 33: Deterministic Model Curves for Various Values of Autocorrelation Lengths Vertical to the Grooves in Valley Parts

2.4 The Quantitative Relation Between ISO Standards

As mentioned in Chapter One, there are ISO standards to describe the liner finishes – ISO 13565-2 and ISO 13565-3. The former one is usually used in liner finish manufacture industry, while the latter one is used as input for surface generation (namely RMS for plateau and valley, and plateau ratio). In order to let industry easily use the surface generation method and study the topology parameters, a quantitative relation between the two standards are developed under the assumption that the valley and plateau parts of the honed surface are both based on normal distribution.

Figure 2.34 shows the connections between height distribution curve and cumulative distribution curve (Abbott Curve). From the curve, the following relations based on the definition of ISO 13565-2 standard can be extracted:

$$\int_{-\infty}^{-0.5R_k*a} \frac{a}{\sqrt{2\pi}\sigma} e^{-\frac{x^2}{2\sigma^2}} dx = M_{r1} \text{ (From Mr1 definition)}$$

$$\int_{-0.2R_k}^{0.2R_k} \frac{a}{\sqrt{2\pi}\sigma} e^{-\frac{x^2}{2\sigma^2}} dx = 0.4 \text{ (From Rk definition)}$$

Where a means plateau ratio, and σ means the RMS for plateau ($sigma_p$). The second equation cannot be broadly used since if plateau ratio of one liner finish is small, the height at $0.2R_k$ is valley part, therefore does not follow the plateau Gaussian distribution. Since the above equation has two unknown variables – plateau ratio and $sigma_p$, another equation is needed to solve the problem. From observation, the following equation is found:

$$\sigma = R_{pk} \text{ (Form observation)}$$

For the valley part, similarly, by the definition, the following equations are found:

$$\int_{-\infty}^{x1} \frac{1}{\sqrt{2\pi}\sigma} e^{-\frac{x^2}{2\sigma^2}} dx = 1 - M_{r2} \text{ (From Mr2 definition)}$$

$$\int_{-\infty}^{x1} \frac{1}{\sqrt{2\pi}\sigma} e^{-\frac{x^2}{2\sigma^2}} (x1 - x) dx = 0.5R_{vk}(1 - M_{r2}) \text{ (From the Rvk definition)}$$

Where x1 is an unknown variable, and σ means the RMS for the valley part ($sigma_v$). Therefore the equation group has two equations and two unknown variables that can be solved numerically.

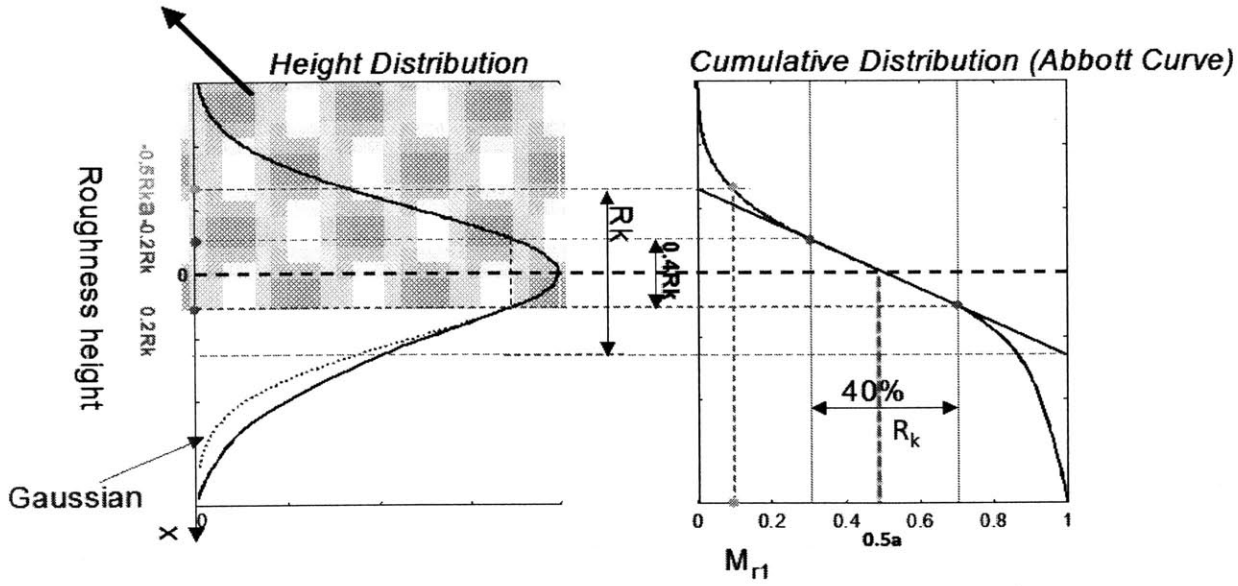

Figure 2. 34: Definition of Rk and Mr1 in Height Distribution Curve

In order to confirm the accuracy of the relations, multiple surfaces (based on liner finish sample 1) with different values of topology parameters are numerically generated. The real value of these topology parameters are compared with the values achieved by the relation we developed.

Figure 2.35 shows the comparison of real values and calculated values. The top left figure shows the different values of $sigma_p$ for multiple liner finishes. The top right figure shows different values of plateau ratio for multiple generated surfaces. The bottom figure shows the various values of $sigma_v$ for generates surfaces. Obviously, the calculated values using the developed relations match well with the real value.

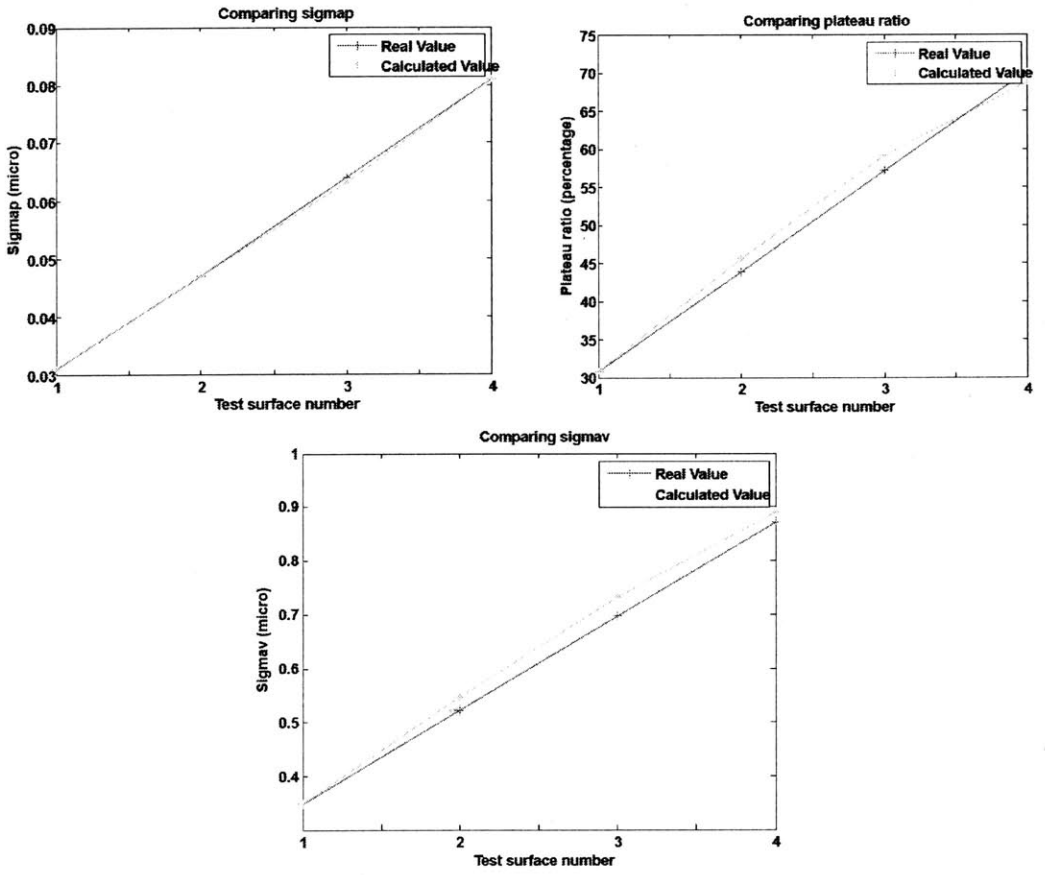

Figure 2. 35: Comparison of Real Values and Calculated Values

A reminder is that ISO 13565-3 standard is only part of the input for the surface generation algorithm. Besides the RMS for plateau and valley, and plateau ratio, the autocorrelation lengths are also very important input variables for the surface

generation method, which cannot be achieved from neither ISO 13565-2 nor 13565-3. As figure 2.36 shown, the autocorrelation lengths do affect the physical behaviors of the liner. If we have the roughness data of the surface, the autocorrelation lengths can be achieved by the methods described in Section One of this Chapter.

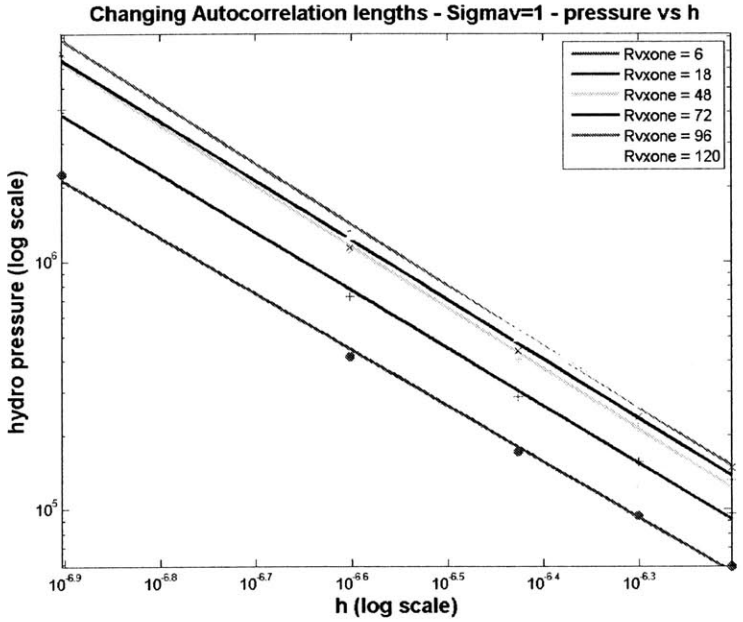

Figure 2. 36: Hydrodynamic Pressure for Multiple Values of Autocorrelation Lengths

2.5 Conclusion

In this chapter, the liner finish generation algorithm is described. Fast Fourier Transform methods are developed to achieve all the input values from the measured surface data (including RMS for plateau and valley, plateau ratio, honing angles, autocorrelation lengths for plateau and valley). Multiple tests are conducted to confirm the reliability of the algorithm. We found that the surface generation algorithm can not only accurately simulate the physical behaviors of the liner finish under engine operation, but also can depress the deviations caused by the measurement error of confocal microscope. The surface generation method is used to study the effects of multiple topology variables on the friction and pressure. Some Quantitative relations can be developed for the deterministic dry contact load and geometric parameters of the plateau. Finally, the quantitative relations between the two ISO standards are developed and tested, so that the manufacture industry can easily use the surface generation algorithm.

3. Honed Liner Finish Wear Process

In this chapter, numerical methods will be used to simulate the break-in processes for honed liner finish. Not only the start and end states, but also the whole processes are simulated based on both measured liner finish and numerically generated liner finish. The friction and pressure behaviors for lightly and heavily worn surfaces are compared with experimental data. Moreover, attempts are made to tune the worn parameters so that the friction effective mean pressure (FMEP) curve can match the experimental data.

3.1 Study Variables for Break-in Processes

As mentioned in Chapter One, there are three parameters can be tuned in the wear process simulation method – cycle, RMS for grinder, and height between the grinder line and mean height of plateau part, where the parameters follows the equations:

$$\sigma_{combined} = \sqrt{{\sigma_p}^2 + {\sigma_g}^2}$$

$$h = const * \sigma_{combined}$$

Where σ_p and σ_g represent the RMS for plateau of the liner and RMS for the grinder line respectively, h is the height between the liner finish and the grinder line. Const is usually chosen to be small enough so that there are interactions between grinder line and liner surface. In this section, we will tune $sigma_g$ (RMS for grinder), const (controlling the height), and cycle to study the effects of these parameters on the friction and pressure. Liner finish sample1 is used as the basic surface (start point).

3.1.1 Wear Process for Measured Surface

First of all, the measured liner finish is used to be the original surface (without worn). $Sigma_g$ is set to be 3e-8m, around half of the value of $sigma_p$. Const is chosen to be 2, and cycle is chosen to be 2, 20, and 200. One needs to pay attention that the cycle here means the number of times the grinder line moves along the liner finish, which is different (but linearly correlated) from the real engine cycle. Figure 3.1 shows the hydrodynamic and dry contact deterministic curves. When the number of cycle changes from 0 to 200, the hydrodynamic pressure almost remains the same, while the hydrodynamic friction and dry contact load obviously decreases. However, from the experimental observation, when the number of cycle is small, hydrodynamic pressure and friction almost remains the same, while dry contact load apparently decreases. As the number of cycle increases to large value, the hydrodynamic part starts to vary. Therefore, the simulation results (especially the hydrodynamic friction) do not match the experimental observation well.

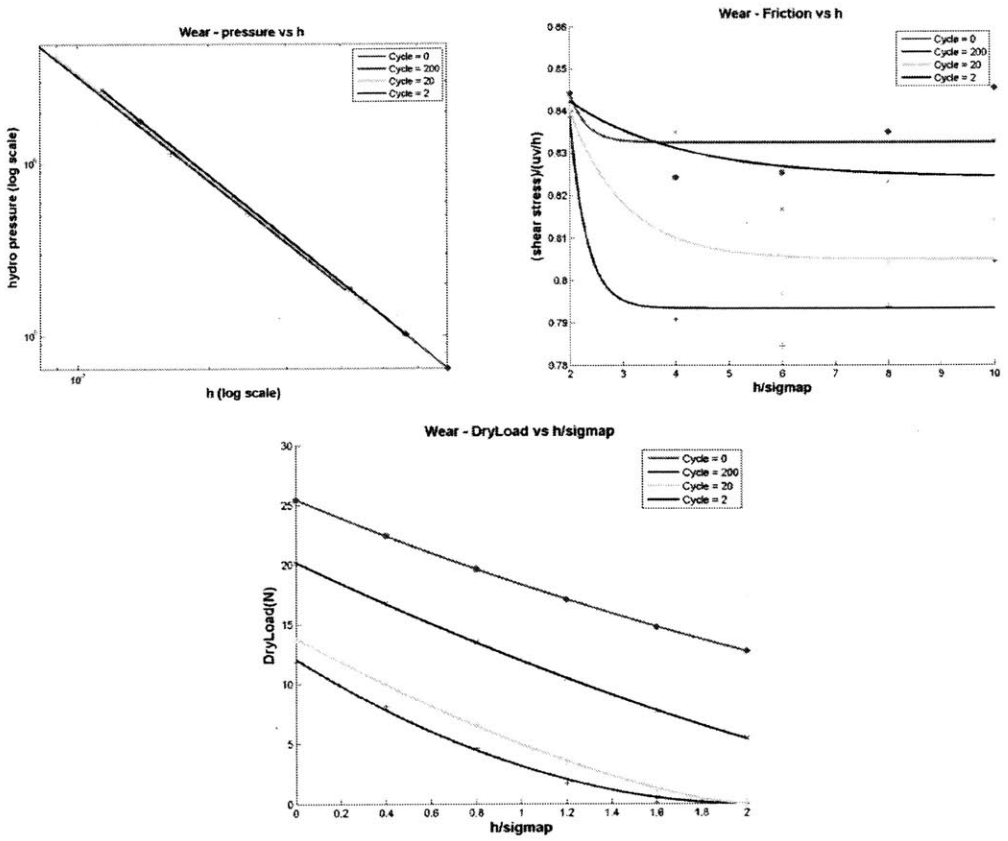

Figure 3. 1: Deterministic Model Curves for sigmag = 3e-08m and const = 2

Since the previous set of variables do not lead to the obvious change of hydrodynamic pressure, either smaller value of const or larger value of $sigma_g$ should be used. First, the simulation is run when const equals 1 and $sigma_g$ equals 3e-08m. Figure 3.2 shows the hydrodynamic deterministic model curves. For the hydrodynamic pressure, when cycle changes from 0 to 20, it almost remains the same. When number of cycle changes from 20 to 200, it decreases. This phenomenon fits the experimental observation. However, the hydrodynamic friction decreases even when cycle changes from 0 to 20, which does not fit the experimental observation.

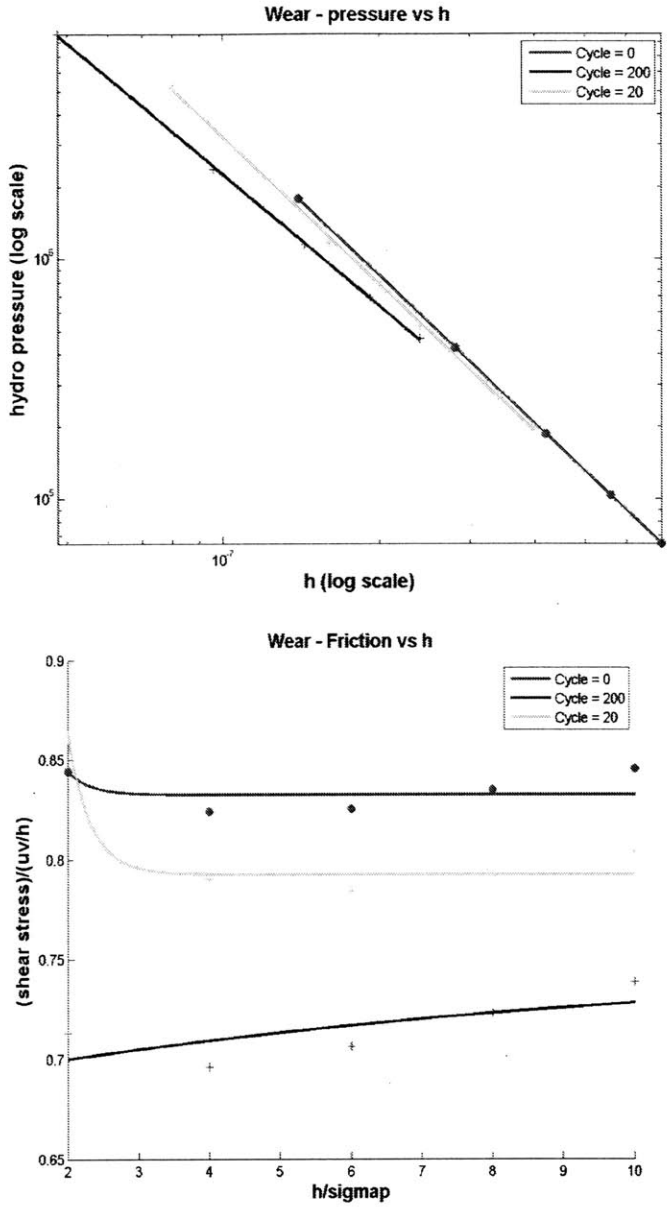

Figure 3. 2: Hydrodynamic Deterministic Model Curves when sigmag = 3e-08m and const = 1

For const equals 2 and $sigma_g$ equals 6e-08m, the hydrodynamic deterministic curve shows in figure 3.3. Similarly, the friction curve drops a lot even with small change of cycle, which do not fit the experimental observations.

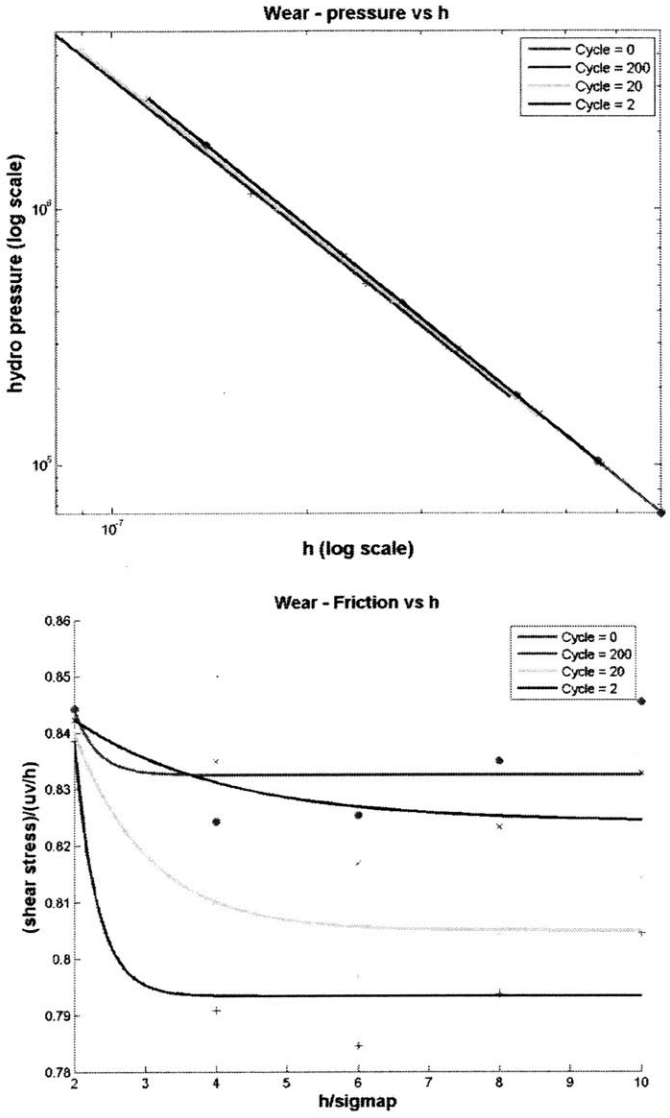

Figure 3. 3: Hydrodynamic Deterministic Model Curves when sigma$_g$ = 6e-08m and const = 2

3.1.2 Wear Process for Generated Surface

The reason for the deviation from experimental observation is that the grinder line removes the fake spikes in the measured liner finish even with small number of cycle. Therefore, the generated surface based on normal distribution is studied and compared with the measured surface.

Figure 3.4 shows the deterministic model curves when $sigma_g$ equals 6e-08m and const equals 2. When the number of cycle is small (2 or 4), the hydrodynamic pressure and friction curves almost remain the same, while the dry contact load obviously drops. When the number of cycle increases to 20 and 40, both the hydrodynamic curves and dry contact ones apparently drop. These phenomenon matches with the experimental observations. Therefore, using the surface worn algorithm based on numerically generated surface can properly simulate the physical behaviors.

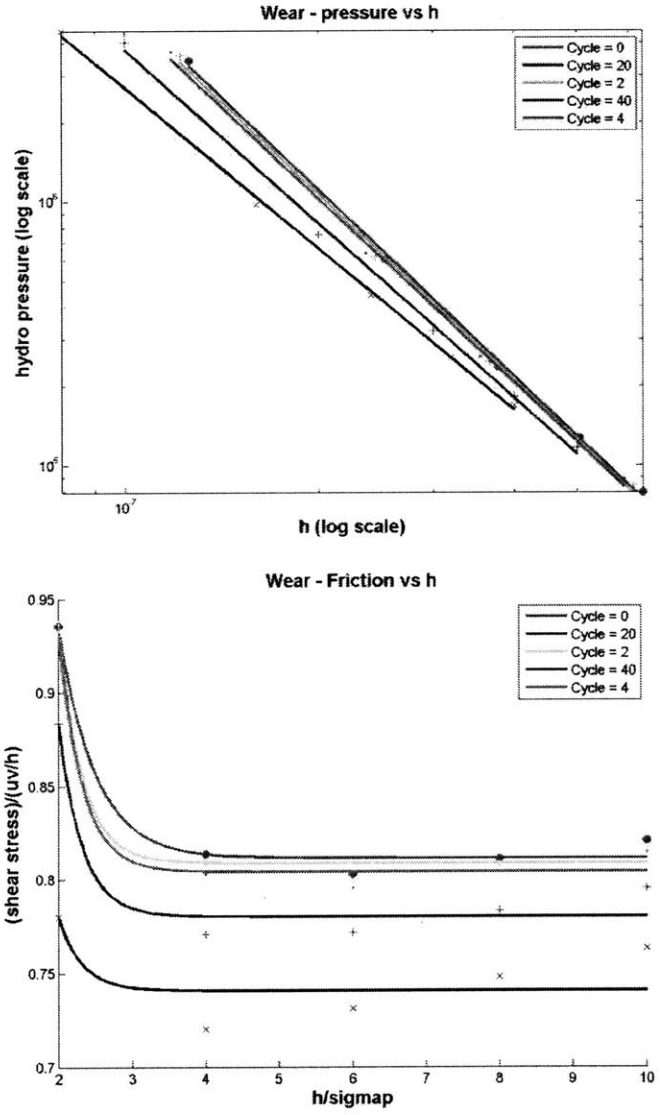

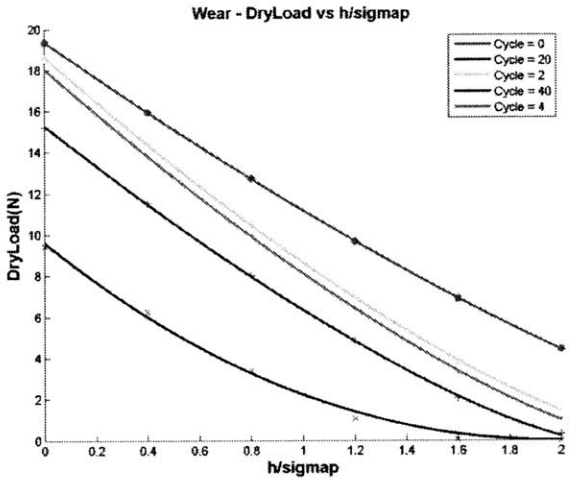

Figure 3. 4: Deterministic Model Curves Based on Generated Surface when $sigma_g$ = 6e-08m and const = 2

In order to further confirm the reliability of the worn surface simulation method, the histogram comparison curves are plotted as figure 3.5 shown. The blue line represents the new surface (namely the numerically generated surface based on sample1), and the green line represents the worn surface when $sigma_g$ equals 3e-08, const equals 2, and cycle equals 10. From the figure, we can find that the difference of histogram mainly happens at the plateau part, matches the real situation.

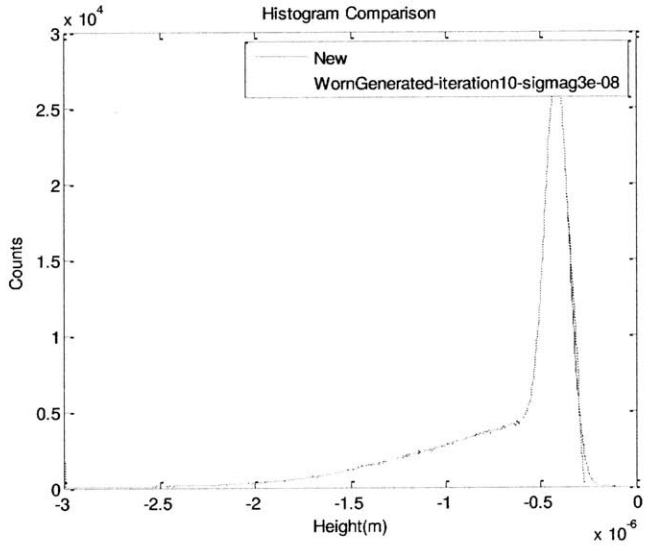

Figure 3. 5: Histogram Comparison of the New Surface and Worn Surface

3.2 Simulation of FMEP Curve

In the break-in process of liner finish, the friction effective mean pressure (FMEP) is an important parameter. Therefore, it is critical that the FMEP curve of the simulated worn surfaces can fit the experimental data (at least the trend is the similar).

Figure 3.6 shows the FMEP curve for the experimental data of liner finish sample 1. It shows that the FMEP value decreases at first when the engine cycle (does not equal to the simulation cycle) is small, then remains stable at a certain value.

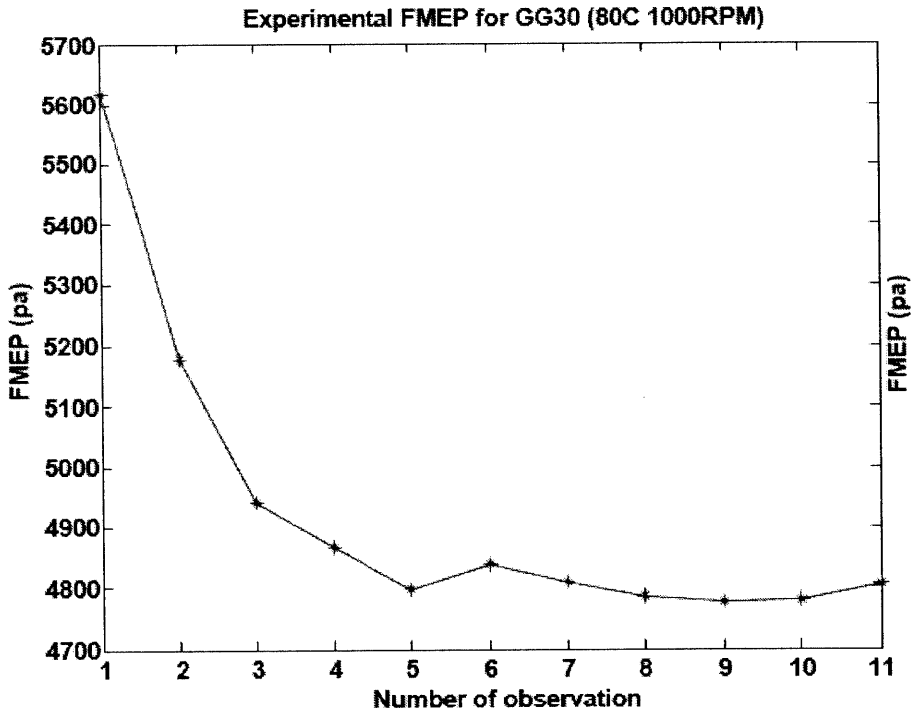

Figure 3. 6: Experimental FMEP Curve for Liner Finish Sample 1

Figure 3.7 shows the simulated FMEP curve when $sigma_g$ equals 6e-08m and const equals 2. The curve decreases at first when the value of cycle is small, and then increases. This does not matches the experimental data. Since the sudden decrease of the curve only happens when cycle is smaller than 5, therefore we should either decrease the value of $sigma_g$ or increase the value of const.

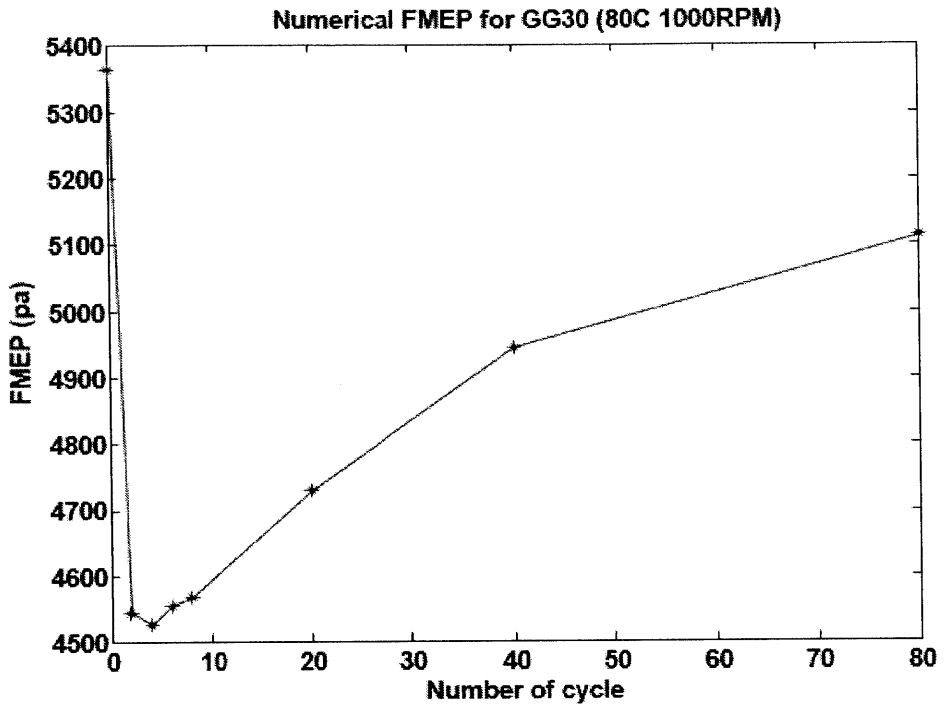

Figure 3. 7: Simulated FMEP Curve when $sigma_g$ = 6e-08m and const = 2

Figure 3.8 shows the simulated FMEP curve when $sigma_g$ equals 3e-08m and const equals 2. The trend of the curve is similar to the experimental data – FMEP decreases at first when the value of cycle is small and then become stable. The difference of the exact values of FMEP is caused by the reason that the roughness data we use for simulation (liner finish sample 1) are the already break-in one, while the experimental data were achieved from the real new to worn liner finishes.

In summary, we can simulate the trend of the FMEP curve by choosing the proper value of the three parameters – $sigma_g$, const, and cycle. In the future, if the new surface roughness data can be achieved, more detailed simulation and tests can be conducted.

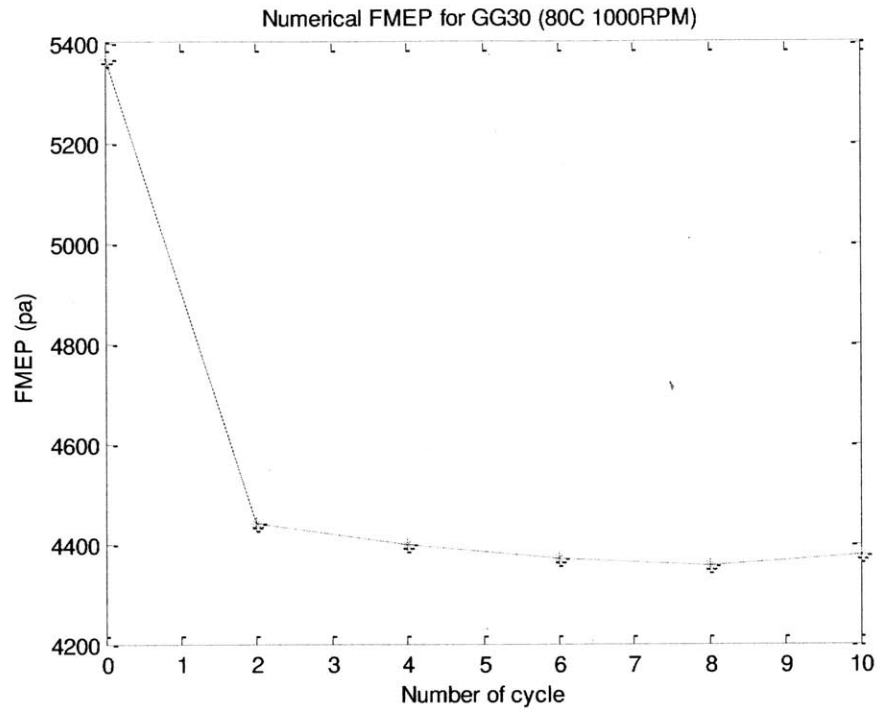

Figure 3. 8: Simulated FMEP Curve when sigma$_g$ = 3e-08m and const = 2

3.3 Conclusion

In this chapter, the surface wear process is simulated. The simulated worn surfaces based on the measured surface do not match the experimental observation when cycle is small due to the great number of fake spikes caused by the confocal microscope.

Since the numerically generated liner finish is based on normal distribution for both the plateau and valley part, it does not have fake spikes. Therefore, the physical behaviors of the simulated worn surfaces based on the generated surface match the experimental observations – when cycle is small, the hydrodynamic part does not change, but the dry contact part changes; when cycle increases, both the hydrodynamic and dry contact part changes.

The trend of the FMEP curve can be simulated by choosing the proper value of the three parameters – sigma$_g$, const, and cycle. In the future, if the new surface roughness data can be achieved, more detailed simulations and tests can be conducted.

4. Sprayed Liner Finish Generation Method

In this chapter, the algorithm to numerically generate thermal sprayed liner finish will be described. The hydrodynamic and dry contact friction behavior for generated surfaces are compared with experimental data. Couple of topology parameters are tuned and their effects on friction losses are studied. Moreover, the effects of the pores created by the plasma spraying processes on the lubrication behavior are simulated.

4.1 Algorithm to Generate Sprayed Liner Finish

In order to numerically generate the liner finish, first we need to calculate the topology parameters from the measured surface, and then use the calculated values as input for the surface generation algorithm.

As mentioned in Chapter one, since the manufacturing processes for thermally sprayed liner finish are different from those for honed liner finish, the roughness distribution of sprayed surface is only based on one normal distribution (for honed surface, both the plateau and valley parts are based on normal distribution, therefore it is a combination of two normal distribution). Therefore, for sprayed surface, the parameters we need is RMS for the surface (sigma_rough), honing angles, and autocorrelation lengths in orthogonal directions. The parameters (except sigma_rough) can be calculated based on the measured surface using the FFT method described in Chapter Two. If we can properly calculate the value of sigma_rough, the surface generation algorithm for the valley part of honed surface (described in Chapter Two) can be used to numerically generate the sprayed surface.

There are two methods to calculate sigma_rough. One is directly using a straight line to fit the scaled material ratio curve of the measured surface. The slope of the line represents sigma_rough. This method can automatically ignore points larger than two sigma, where most points belong to the fake spikes. Figure 4.1 shows the histogram of the measured surface and the generated surface based on this method. It appears that the two histograms do not match with each other, indicating that the calculated sigma_rough value deviates from the real one. The reason for the deviation is probably that there are great number of fake spikes with height less than two sigma_rough, which are included by the scaled materials ratio curve.

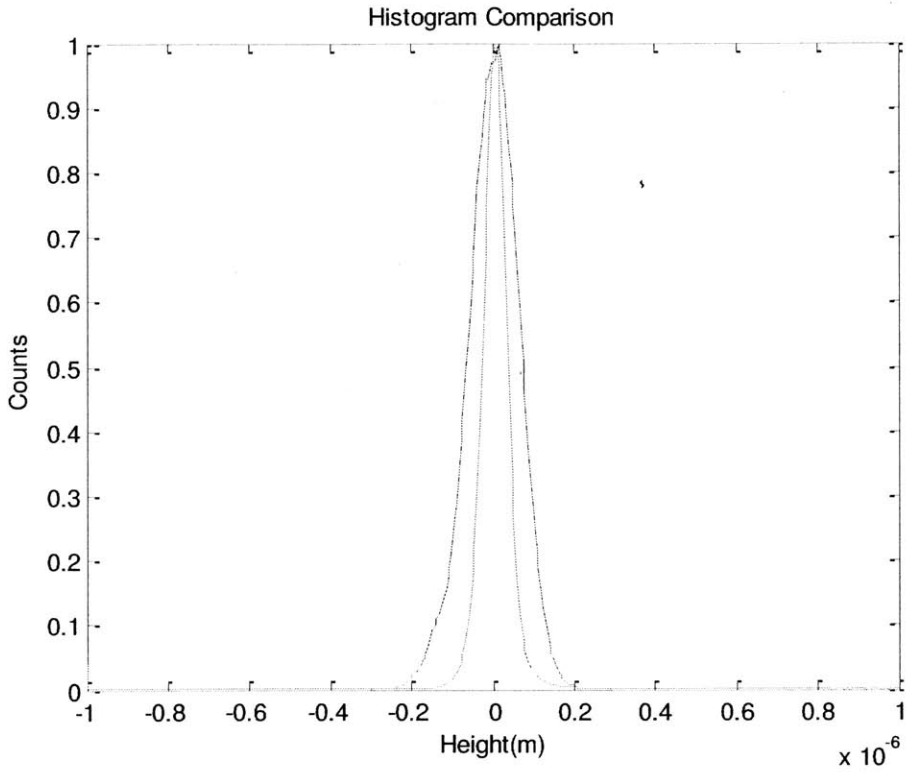

Figure 4. 1: Histogram of the Measured Surface and the Generated Surface Using the sigma_rough Calculated by the Scaled Material Ratio Curve

Another way to calculate the value of sigma_rough is directly fitting the histogram. Since the sprayed liner finish is only based on one normal distribution, the fitting algorithm is simple. First of all, we find the peak of the histogram for measured surface. Then the point with counts equals to half of the peak is found. The height difference between the peak and the point can be calculated, and finally the corresponding sigma_rough can be achieved. Figure 4.2 shows the histograms of the measured surface and the numerically generated surface based on sigma_rough calculated by this method. The two histogram matches with each other. Therefore, this method should be better compared with the previous one. In the next section, both methods will be compared with experimental data to further confirm the point.

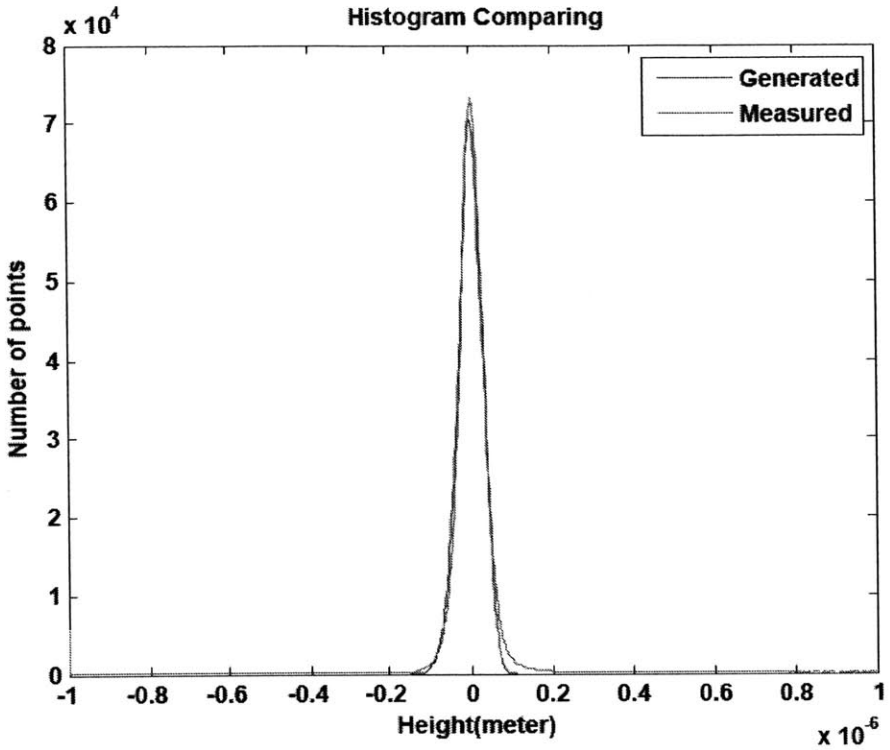

Figure 4. 2: Histogram of the Measured Surface and the Generated Surface Using the sigma_rough Calculated by Directly Fitting the Histograms

Figure 4.3 concludes the basic steps to calculate the topology parameters of the sprayed liner finish, which are used as input for the surface generation algorithm.

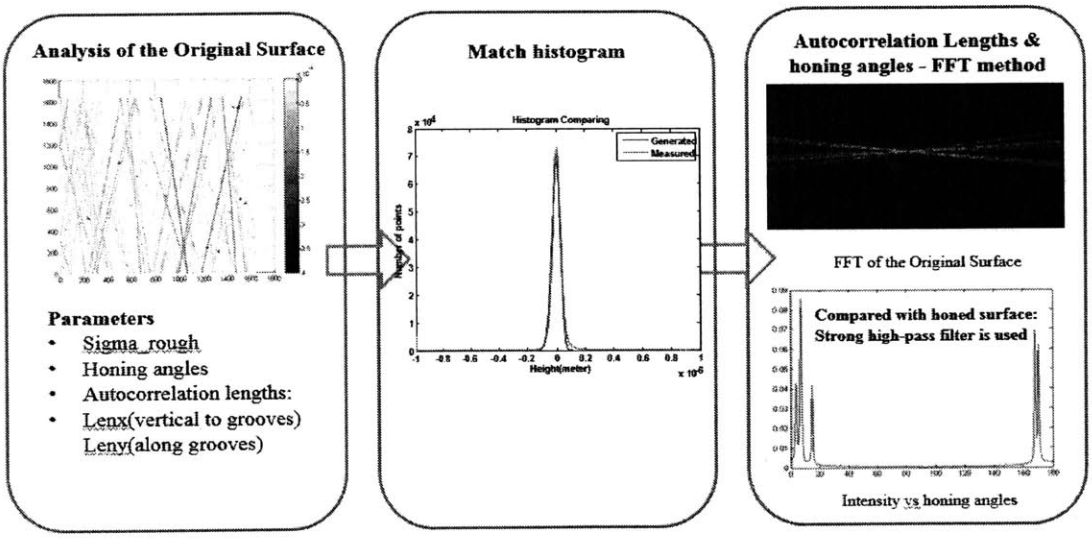

Figure 4. 3: Basic Steps to Calculate the Topology Parameters of Sprayed Liner Finish

4.2 Test of the Sprayed Surface Generation Method

In this section, the generated surfaces will be put into the deterministic models and cycle model, and their physical behaviors will be compared with the experimental data to test the accuracy of the method. The reference surface is called liner finish sample 3. The measured roughness data is shown in Figure 4.4.

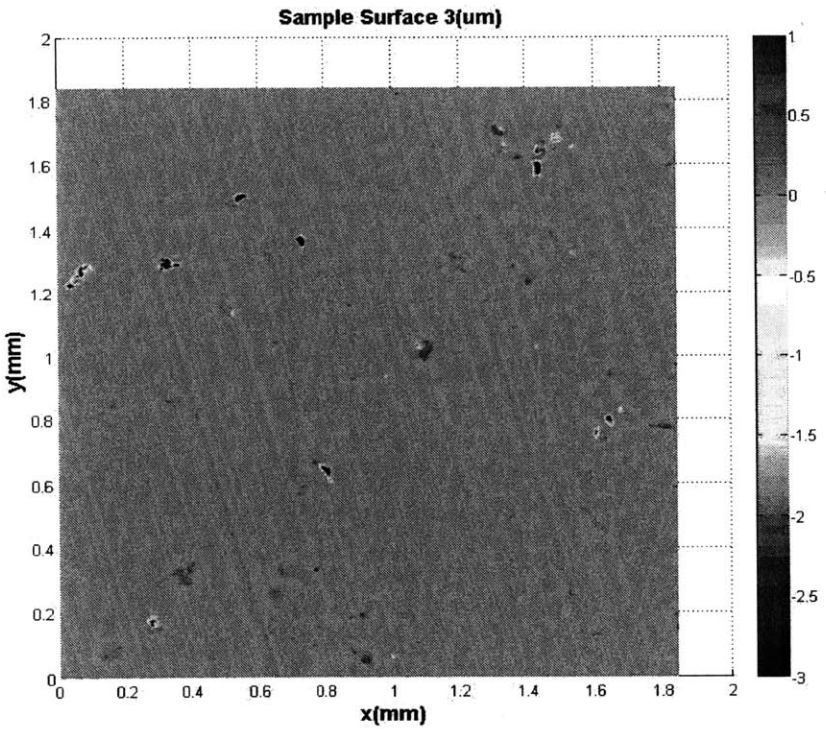

Figure 4. 4: Measured Sprayed Liner Finish Sample 3

Using the algorithm described in the previously section, we can numerically generate the surface. Figure 4.5 shows the roughness data of the generated surface with sigma_rough calculated by directly fitting the histogram. Compared with the measured surface, it is obvious that the generated one does not have the pores caused by the thermally spray processes. We directly extract the pores from the measured surface and add them to the generated surface (as figure 4.6 shown), so that the functions of the pores can be studied.

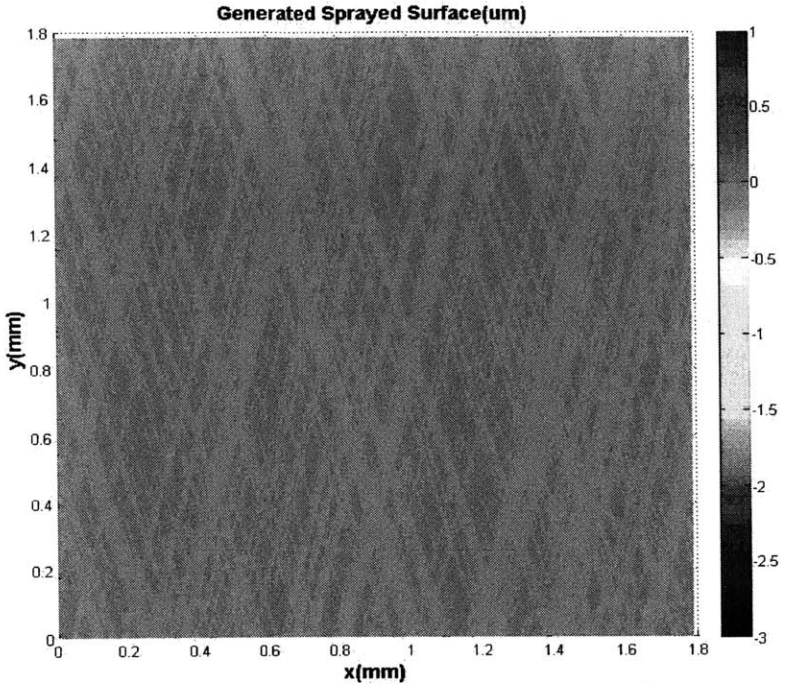

Figure 4. 5: Numerically Generated Sprayed Surface with sigma_rough Calculated by Fitting the Histogram

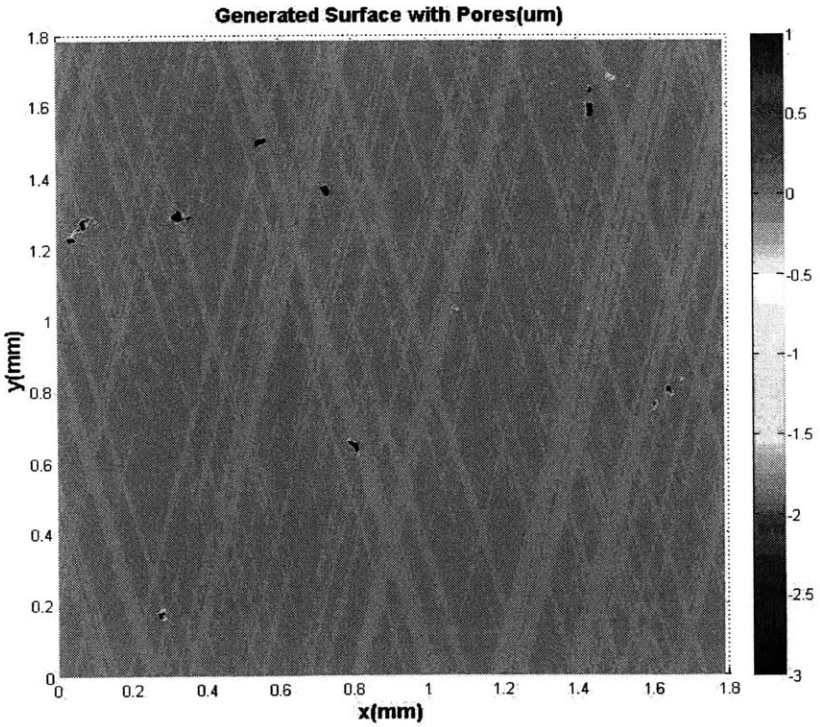

Figure 4. 6: Numerically Generated Sprayed Surface with Pores

The measured surface and the generated ones are firstly inputted into the hydrodynamic and dry contact deterministic models. Figure 4.7 shows the deterministic model curves. The red line represents the measured surface. The green line represents the generated surface using the value of sigma_rough calculated by fitting the histogram and with pores. This line fits the experimental well in the hydrodynamic part. The reason for the deviation in the dry contact part is that there are large number of fake spikes existing in the measured surface. The deterministic dry contact model is very sensitive to the spikes. The blue line represents the generated surface with the same method to calculate sigma_rough but without pores. The blue line is almost covered by the green line in both hydrodynamic and dry contact parts, indicating that the pores do not have obvious function for lubrication. This is conflicted with the common belief that the pores improve the oil retention ability of the liner finish. The black line represents the generated surface with sigma_rough calculated by the scaled material ratio curve. It deviates in both hydrodynamic and dry contact parts, indicating that the method to fit histogram is better. It is clear that larger sigma_rough (in the figure sigmap represents sigma_rough) leads to lower hydrodynamic friction coefficient, which means smaller friction is created under the same pressure. In contrast, larger value of sigma_rough causes obviously increase of dry contact load, which leads higher dry contact friction losses.

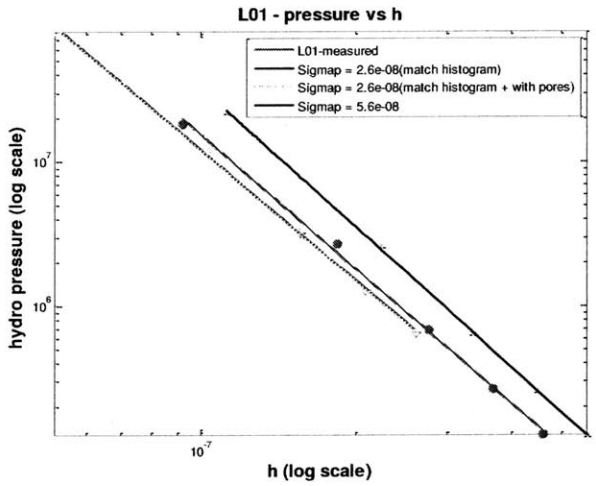

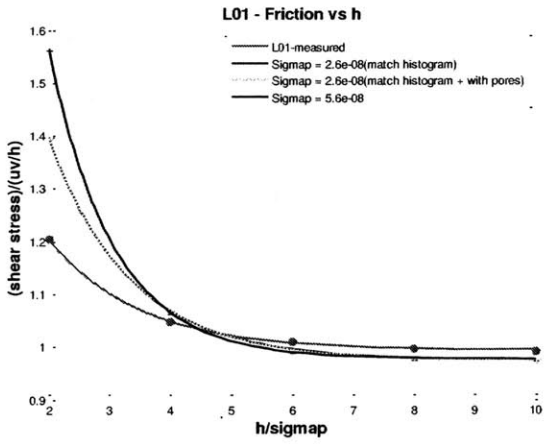

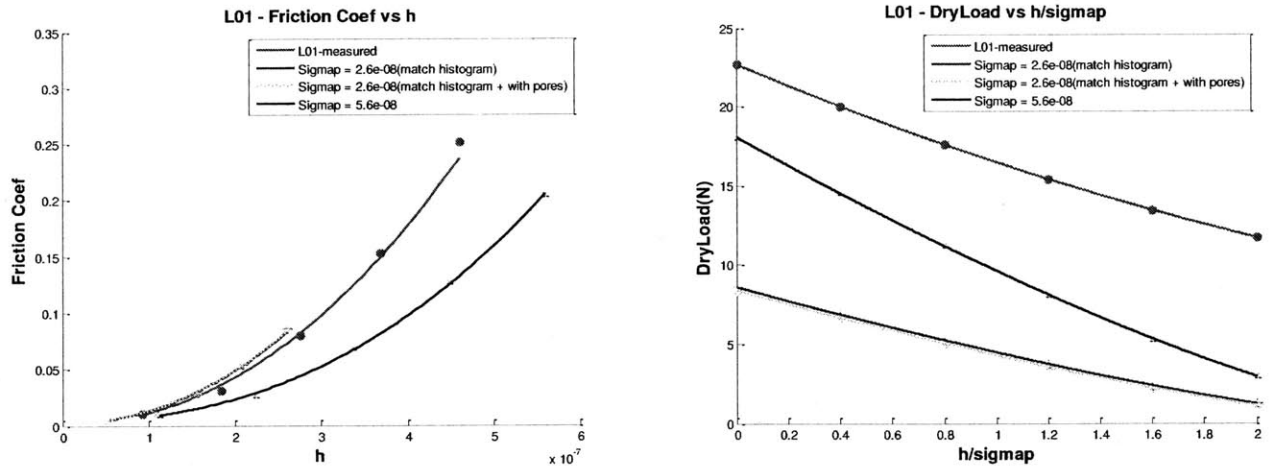

Figure 4. 7: Deterministic Model Curves for the Measured and Generated Liner Finishes

The deterministic parameters are then used in the engine cycle model. Figure 4.8 shows the friction curves when temperature is 40C and the speed is 500RPM. The experimental data is shown as the blue line. From the shape of the curve around the center, we can conclude that it is hydrodynamic behavior dominated. The green line represents the generated surface, which fits the experimental data, indicating that the surface generation method is able to duplicate the hydrodynamic behavior of sprayed surfaces. The red dash line represents the simulation results using the measured surface, which deviates from the experimental data. The reason for the deviation is that the fake spikes cause much larger dry contact load parameters, which significantly increase the friction in the cycle model.

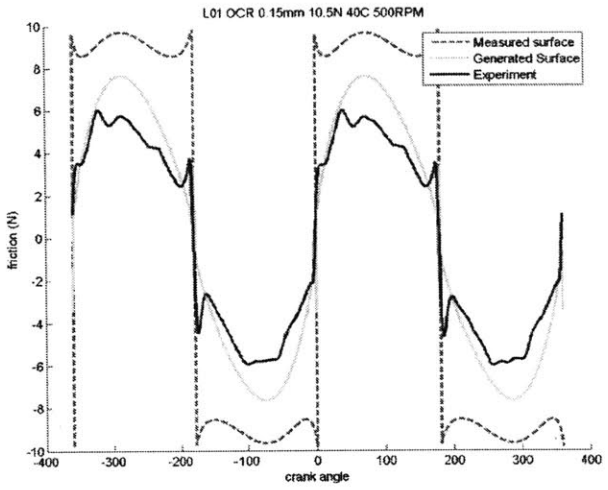

Figure 4. 8: Cycle Model Curves When Temperature is 40C and speed is 500RPM

Figure 4.9 shows the friction curves when temperature is 40C and the speed is 100RPM. The experimental data is shown as the blue line. From the shape of the curve around the center, we can conclude that it is a combination of hydrodynamic and dry contact behaviors. The green line represents the numerically generated surface, which deviates a little from the experimental data, which indicates that the dry contact load is smaller than the real value. The possible reason for the deviation is that the surface is generated based on one normal distribution, but for real situation, the liner finish might deviate from the normal one. Therefore, more dedicated surface generation method should be developed to simulate the dry contact behaviors. The red dash line represents the simulation results using the measured surface as input, which apparently deviates from the experimental data, indicating that the fake spikes lead to much higher dry contact load.

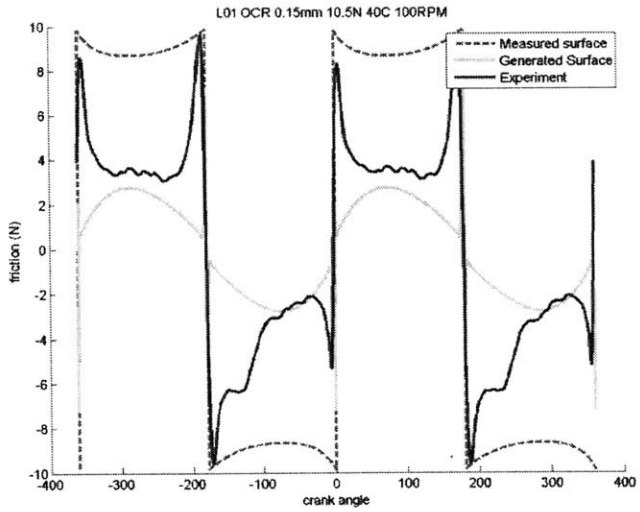

Figure 4. 9: Cycle Model Curves When Temperature is 40C and speed is 100RPM

4.3 Topological Parameters of Sprayed Surface

Sigma_rough is a critical topological parameter to the physical behaviors of the liner finish. As the previous section shown, when sigma_rough increases, the hydrodynamic frication coefficient decreases, while the dry contact load increases. Therefore it is a tradeoff between hydro friction losses and dry contact losses. In this section, more values of sigma_rough is simulated to reconfirm this statement.

Figure 4.10 shows the deterministic model curves for various values of sigma_rough. It is obvious that larger value of sigma_rough leads to larger hydrodynamic pressure, lower friction coefficient. Meanwhile, the dry contact load significantly increases. One thing necessary to emphasize is that when the simulated sprayed liner finish with large value of sigma_rough (larger than 0.1 micrometer) is similar to the valley part of honed surface, which has higher hydro pressure compared with normal sprayed surface. Therefore, the larger hydro pressure of sprayed surface (compared with honed surface) is not due to the pores. In fact, the plateau honing process decreases the hydro pressure of honed surface. The reason for this process is to achieve fine plateau that can depress the dry contact load. All in all, for all liner finishes, a tradeoff should be made between less hydro pressure and less dry contact load.

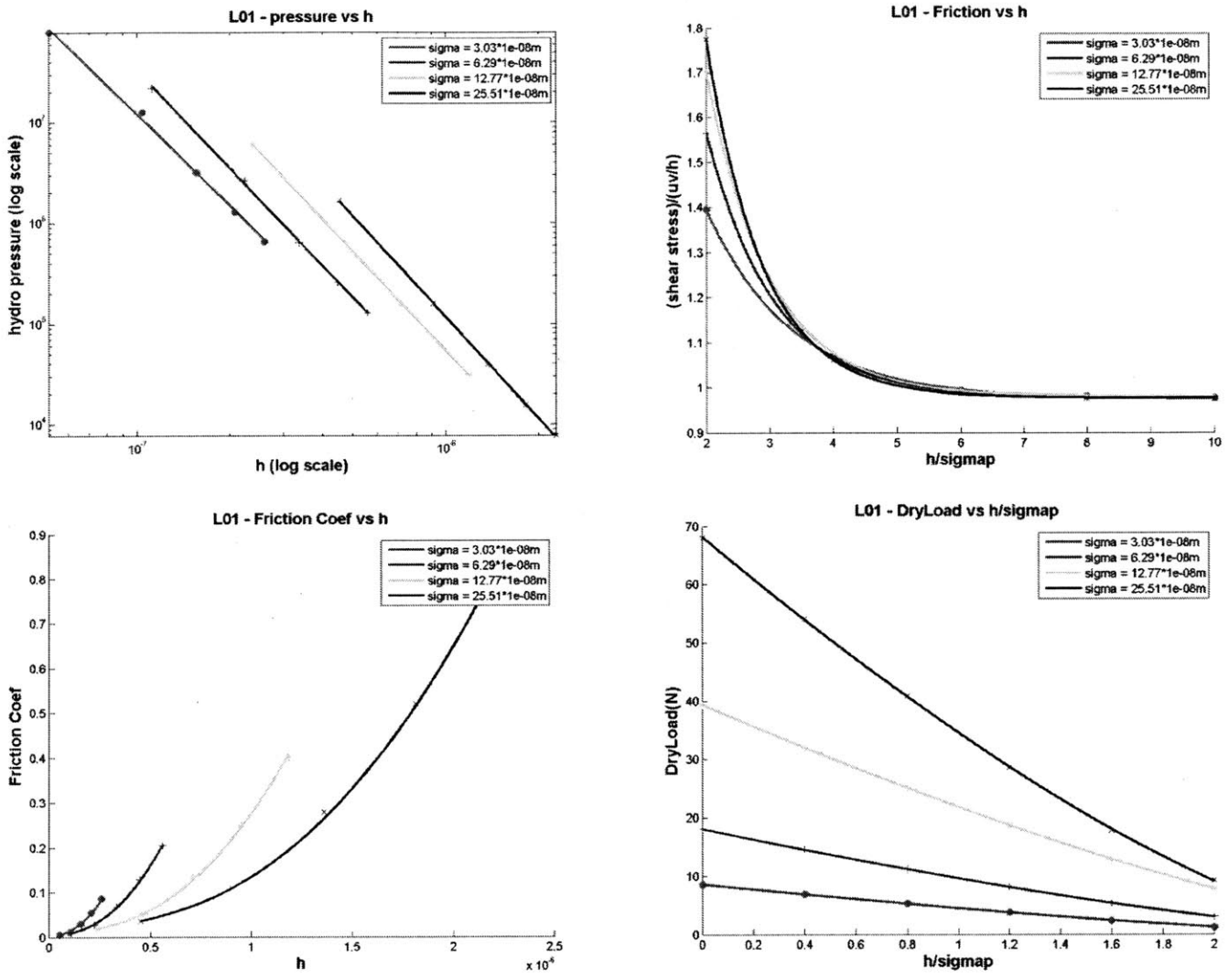

Figure 4. 10: Deterministic Model Curves for Various Values of Sigma_rough

Besides sigma_rough, autocorrelation length of sprayed liner finish is also a critical parameter that affects the physical behaviors of the surface. The value of autocorrelation length vertical to the grooves relates to the width of the grooves. Larger values of autocorrelation length vertical to the grooves lead to wider grooves.

Figure 4.11 shows the deterministic model curves with multiple values of autocorrelation lengths. The figure shows that larger values of autocorrelation lengths (wider grooves) lead to lower hydrodynamic friction and lower dry contact load.

Therefore, when sigma_rough is fixed, one should try to manufacture sprayed liner finish with wider grooves to achieve lower friction losses.

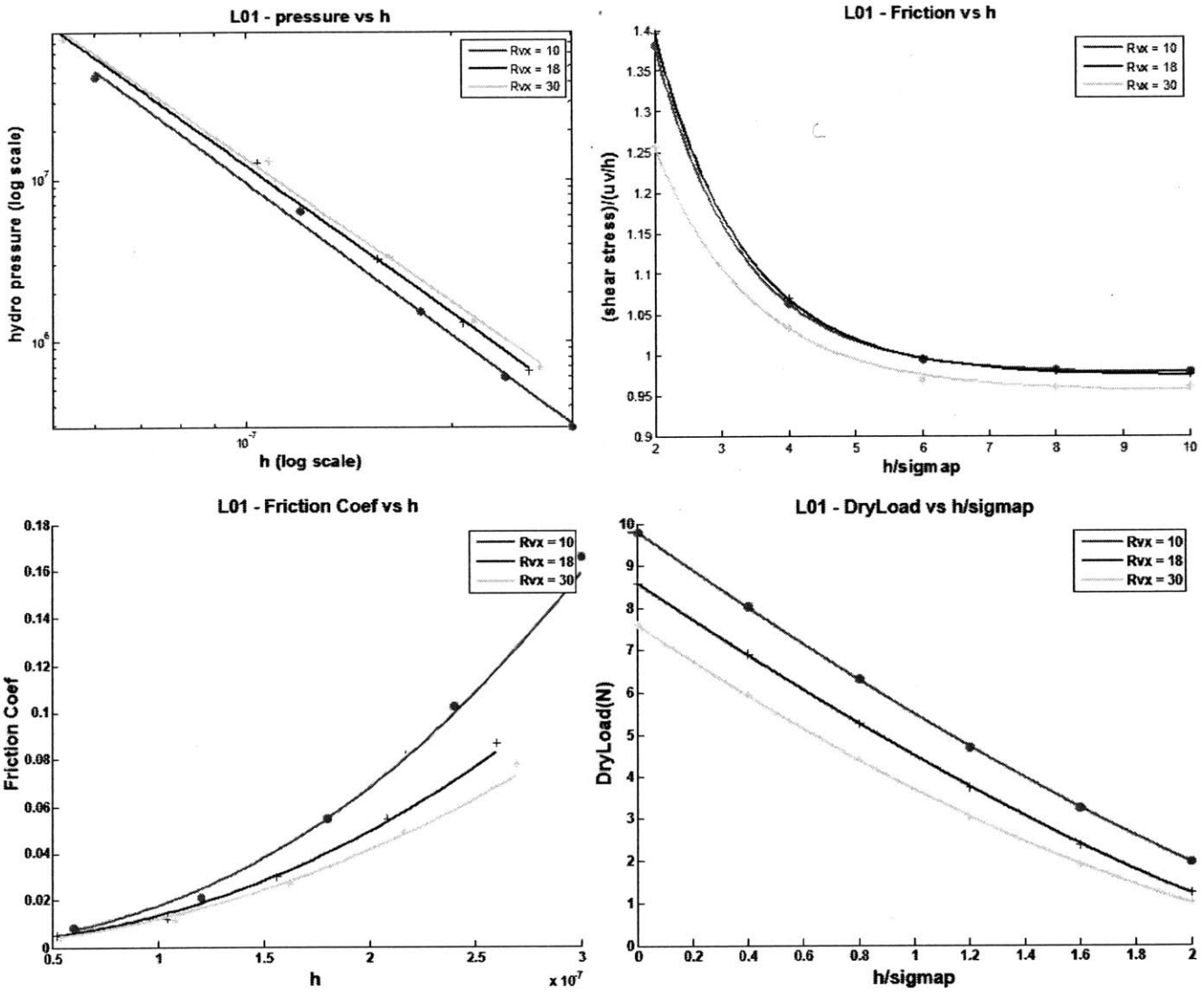

Figure 4. 11: Deterministic Model Curves for Multiple Values of Autocorrelation Lengths

4.4 Conclusion

In this chapter, the method to numerically generate sprayed liner finish is described. The method can effectively avoid the fake spikes existing in the measured surface

caused by confocal microscope. By comparing with experimental data, it is confirmed that the hydrodynamic behaviors can be accurately simulated by the method, while the dry contact part needs further modification. We found that the pores caused by the thermally sprayed processes do not have obvious effects on the lubrication behavior. Finally, we study the topology parameter – autocorrelation length. It is found that larger value of autocorrelation length (therefore wider grooves) lead to smaller friction losses in both hydrodynamic and dry contact parts.

5. Conclusion

5.1 Summary and Conclusion

The objective of this thesis is to use numerical methods to generate liner finishes based on certain topology parameters. The generated surface should be able to simulate the lubrication and dry contact behaviors of the original surface, so that people are able to use this method to study the effects of various topology parameters on friction losses.

For the two-step honed liner finish, the surface generation method has already been existing. In this research, Fast Fourier Transform methods are developed to obtain all the input values for the surface generation method (including RMS of plateau and valley, plateau ratio, honing angles, autocorrelation lengths of plateau and valley). Multiple tests are conducted to confirm the reliability of the algorithm. We found that the surface generation algorithm can not only accurately simulate the physical behaviors of the liner finish under engine operation, but also depress the deviations caused by the measurement error of confocal microscope. The surface generation method is used to study the effects of multiple topology variables on the friction and the pressure. Some Quantitative relations has been developed for the deterministic dry contact load and geometric parameters of the plateau. The quantitative relations between the two ISO standards (ISO 13565-2 and 13565-3 standards) are developed and tested, so that the manufacture industry can easily use the surface generation algorithm.

For the wear process of honed liner finishes, the simulation method is described. The simulated worn surfaces based on the measured surface do not match the experimental observation when cycle is small due to the great number of fake spikes caused by the confocal microscope. Since the numerically generated liner finish is based on normal distribution for both the plateau and the valley part, it does not have fake spikes. Therefore, the physical behaviors of the simulated worn surfaces based on the

generated surface matched the experimental observations – when cycle is small, the hydrodynamic part does not change, but the dry contact part changes; as cycle increases, both the hydrodynamic and the dry contact part change. The trend of the FMEP curve can be simulated by choosing the proper values of the three parameters – $sigma_g$, const, and cycle.

For the thermally sprayed liner finish, the methods to analyze the original surfaces (by fitting the histograms) and to numerically generate surfaces are described. The method can effectively avoid the fake spikes existing in the measured surface caused by confocal microscope. By comparing with experimental data, it is confirmed that the hydrodynamic behaviors can be accurately simulated with the method, while the dry contact part needs further modification. We found that the pores caused by the thermally sprayed processes do not have obvious effects on the lubrication behavior. Finally, we study the topological parameter – autocorrelation length. It has been found that larger value of autocorrelation length (therefore wider grooves) lead to smaller friction losses in both hydrodynamic and dry contact parts.

5.2 Potential Future Work

For the honed liner finish, detailed study of the topology parameters can be conducted. The reasons why the change of certain parameters leads to either increase or decrease in friction can be explored. Moreover, the comprehensive optimization of the parameters to achieve less friction losses and less oil consumption can be conducted.

For the surface break-in simulation, the current method is based on statistical assumptions. The physical reaction during the interaction between the grinder surface and the plateau needs to be studied. Furthermore, in the thesis, the parameters – const, cycle, and $sigma_g$ is artificially set. In future work, methods should be developed to automatically set the parameters so that the simulation can match the real break-in processes.

For the thermally sprayed surface, more dedicated method should be developed so that not only the lubrication part, but also the dry contact part can be matched with the experimental data. The reasons for the high hydrodynamic pressure should be studied. Moreover, effects of other topology parameters like the honing angles can be studied.

Reference

[1] Richardson, D.E., "Review of Power Cylinder Friction for Diesel Engines", ASME Journal of Engineering for Gas Turbines and Power, 122, 506-519, 2000.

[2] R. Reizer, and P. Pawlus, "Modelling of plateau honed cylinder surface topography," Proceedings of the Institution of Mechanical Engineers, Part B: Journal of Engineering Manufacture, 1564-1578, 2012.

[3] Liao, K., Chen, H., Tian, T. "The Study of Friction between Piston Ring and Different Cylinder Liners using Floating Liner Engine - Part 1," SAE Technical Paper, 2012-01-1334, 2012.

[4] Chen H., "Modeling of Liner Finish Effects on Oil Control Ring Lubrication in Internal Combustion Engines Based on Deterministic Method", Master Thesis, Massachusetts Institute of Technology, Cambridge, USA, 2008.

[5] Chen, H., Liao, K., Tian, T., "A Numerical and Experimental Study of Twin-land Oil Control Ring Friction in Internal Combustion Engines Part 2," SAE Technical Paper, 2012-01-1321, 2012.

[6] Li, Y., Chen, H. and Tian, T., "A deterministic model for lubricant transport within complex geometry under sliding contact and its application in the interaction between the oil control ring and rough liner in internal combustion engines", SAE International Powertrains, Fuels and Lubricants Congress, SAE2008-01-1615, 2008.

[7] Liao, K., Liu, Y., Kim, D., Urzua, P., & Tian, T., "Practical challenges in determining piston ring friction", Proceedings of the Institution of Mechanical Engineers, Part J: Journal of Engineering Tribology 227(2), 112-125, 2013.

[8] Liao, K, "Factors Affecting Piston Ring Friction", Ph.D. thesis, Massachusetts Institute of Technology, Cambridge, USA, 2013.

[9] Tian, T., "Modeling the Performance of the Piston Ring-Pack in Internal Combustion Engines", Ph.D. thesis, Department of Mechanical Engineering, MIT, Boston, MA, 1997.

[10] Yang Liu, "Developing an Approach Utilizing Local Deterministic Analysis to Predict the Cycle Friction of the Piston Ring-pack in Internal Combustion Engines", Master thesis, Massachusetts Institute of Technology, Cambridge, USA, 2013.

[11] Pawel Pawlus, "Simulation of stratified surface topographies", Wear, 264, 457–463, 2008.

[12] J. Wu, "Simulation of rough surfaces with FFT," Tribology International, 47-58, 2000.

[13] V. Bakolas, "Numerical generation of arbitrarily oriented non-Gaussian three-dimensional rough surfaces," Wear, 546–554, 2003.

[14] Etienne Decencière, Dominique Jeulin, "Morphological decomposition of the surface topography of an internal combustion engine cylinder to characterize wear", Wear, 482-488, 2001.

[15] Burscheid, "Piston Ring Handbook", Federal-Mogul Burscheid GmbH, August 2008.
[16] L. Sabri, S.Mezghani, M. El Mansori, H. Zahouani, "Multiscale Study of Finish-Honing Process in Mass Production of Cylinder Liner", Wear, March 2010.
[17] D. Lawrence, "An Accurate and Robust Method for the Honing Angle Evaluation of Cylinder Liner Surface Using Machine Vision", Int. J. Adv. Manuf. Technol., 2011.
[18] Qing Zhao, "Modeling of Contact between Liner Finish and Piston Ring in Internal Combustion Engines Based on 3D Measured Surface", Master thesis, Massachusetts Institute of Technology, Cambridge, USA, 2014.
[19] C. Anderberg, P. Pawlus, B.-G. Rosén, T.R. Thomas, "Alternative descriptions of roughness for cylinder liner production", Journal of Materials Processing Technology 209, 1936-1942, 2009.
[20] P Pawlus, R Reizer, A Lenart, "Comparison of parameters describing stratified surface topography", Journal of Physics: Conference Series 483, 012021, 2014.
[21] Kumar, R., Kumar, S., Prakash, B., Sethuramiah, A., "Assessment of engine liner wear from bearing area curves", Wear, 239, 282–286, 2000.
[22] Mainsah, E., Greenwood, J.A., Chetwynd, D.G. (Eds.), "Metrology and Properties of Engineering Surfaces", Springer-Verlag, Berlin, 2001.
[23] Malburg, M.C., Raja, J., "Characterisation of surface texture generated by plateau honing process" Ann. CIRP, 42, 637–639, 1993.
[24] Bohm H J, International Journal of Machine Tools and Manufacture, 32, 109-113, 1992.
[25] Newland DE, "An introduction to random vibration and spectral analysis", 2nd ed. London: Longman, 1984.
[26] T. V. Vorburger, H. G. Rhee, T. B. Renegar, J. F. Song, A. Zheng, "Comparison of Optical and Stylus Methods for Measurement of Surface Texture", Int. J. Adv. Manuf. Technol., 2007.
[27] J. F. Song, T. V. Vorburger, "Stylus Profiling at High Resolution and Low Force", Applied Optics, 1991.
[28] D. H. Lee, N. G. Cho, "Assessment of Surface Profile Data Acquired by a Stylus Profilometer", Measurement and Science Technology, 2012.
[29] D. K. Hamilton, T. Wilson, "Three-Dimensional Surface Measurement Using the Confocal Scanning Microscope", Applied Physics B, 1982.
[30] D. A. Lange, H. M. Jennings, S. P. Shah, "Analysis of Surface Roughness Using Confocal Microscopy", Journal of materials science, 1993.
[31] D. Semwogerere, E. R. Weeks, "Confocal Microscopy", Encyclopedia of Biomaterials and Biomedical Engineering, 2013.
[32] P. Pavlicek, O. Hybl, "White-Light Interferometry on Rough Surfaces---Measurement Uncertainty Caused by Surface Roughness", Applied Optics, 2008.

[33] P. Sandoz, R. Devillers, A. Plata, "Unambiguous Profilometry by Fringe- Order Identification in White-Light Phase-Shifting Interferometry", Journal of Modern Optics, July 2009.

[34] H. J. Jordan, M. Wegner, H. Tiziani, "Highly Accurate Non-Contact Characterization of Engineering Surfaces Using Confocal Microscopy", Measurements and Science Technology, 1998.

[35] Barbezat, G., "Application of thermal spraying in the automobile industry", Surface &Coatings Technology 201, 2028-2031, 2006.

[36] Barbezat, G., "Thermal spray coatings for tribological applications in the automotive industry", Advanced Engineering Materials 8 No. 7, 678-681, 2006.

[37] Ernst, P., Barbezat, G., "Thermal spray applications in powertrain contribute to the saving of energy and materials resources", Surface & Coatings Technology 202, 4428-4431, 2008.

[38] Peter Ernst and Kevin Fletcher, "SUMEBore – thermally sprayed protective coatings for cylinder liner surfaces", Thermal Spray Bulletin, 2012.

[39] Gerard Barbezat, 'Advanced thermal spray technology and coating for lightweight engine blocks for the automotive industry', Surface and Coatings Technology 200, 1990-1993, 2005.

[40] C. H. Venner, A. A. Lubrecht, "Multilevel Methods in Lubrication", Elsevier Science, 2000.

[41] Zachary Westerfield, Master Thesis, Massachusetts Institute of Technology, Cambridge, USA, 2015.